Lower Limb Muscle-Tendon Unit Properties in Human Locomotion

by

Alex N. Denton

A dissertation submitted in partial fulfillment
of the requirements for the degree of
Doctor of Philosophy
(Movement Science)
in the University of Michigan
2023

Doctoral Committee:

Professor Brian R. Umberger, Chair
Associate Professor Robert D. Gregg
Associate Professor Melissa M. Gross
Associate Professor David B. Lipps

Alex N. Denton

alxdent@umich.edu

ORCID iD: 0000-0002-4939-4819

Dedication

For my parents, Craig and Joy.

Acknowledgments

I would like to express my sincere gratitude and appreciation to those who have guided, supported, and encouraged me throughout the course of this dissertation and my time at the University of Michigan.

To my mentor, Brian, thank you for the amazing opportunity to pursue doctoral and master's degrees under your guidance. Your mentorship and support over these last five years is invaluable. It has been an honor to be your first doctoral student at the University of Michigan.

To my dissertation committee, David Lipps, Melissa Gross, and Bobby Gregg, this work would not be possible without your expertise, support, and counsel through every step of the process. Thank you for serving on my committee and being open to my ideas.

To my lab mates in the Locomotion Laboratory, both past and present, thank you for your motivation and assistance along the way, but most importantly your friendship. This work would not be complete without your support.

To my partner, Bryce, I could not wish for better a companion. You always encourage me to pursue my dreams. Thank for you solving the two-body problem and for your unwavering support.

Preface

The chapters of this dissertation have been written as separate manuscripts for submission. Chapter Two has been submitted to the *International Journal for Numerical Methods in Biomedical Engineering.* Chapters Three and Four are in preparation for submission.

Table of Contents

List of Figures

List of Tables

Abstract

The muscle-tendon unit (MTU) is the motor responsible for voluntary movement. Biomechanical properties of muscles and tendons can change over the lifespan in response to aging, disease, and physical training. The impact of MTU biomechanical properties on musculoskeletal function is poorly understood but has broad implications for understanding a range of phenomena including clinical gait disorders, human performance, and the evolution of human bipedalism.

The purpose of this dissertation was to explore the properties of lower limb MTUs and better understand how they influence the mechanics and metabolic energy cost of human locomotion. We used a musculoskeletal modeling approach in isolation, and integrated with experimental techniques. It is challenging to investigate human MTU properties *in vivo*, but they are readily modifiable in a musculoskeletal model and can be isolated from confounding factors. The computational demands of biomechanical simulation present substantial limitations, but modern computers with multicore processors can potentially overcome these limitations through parallel computing. Thus, the first study of this dissertation focused on achieving the computational performance necessary to meet the demands of the remaining two studies.

In Chapter 2, we analyzed the parallel speed-up in solving optimal control simulations of human movement using multicore parallel computing. The results suggest up to a several-fold speed-up can be achieved across a range of musculoskeletal simulations; however, the actual performance improvement is problem specific and requires careful evaluation. This knowledge

was used to facilitate the large number of simulations performed in Chapters 3 and 4 of this dissertation.

In Chapter 3, we used musculoskeletal simulation to investigate the effects of optimal muscle fiber length, tendon slack length, and tendon stiffness on whole-body and muscle-specific locomotor performance. We found lower limb MTU properties can be optimized to reduce whole-body neuromuscular and metabolic demands of human walking. However, reducing overall demands typically required increased effort or cost in some muscles that were offset by greater reductions in others. These MTU-specific performance outcomes may reflect evolutionary trade-offs associated with the need to perform tasks besides level walking.

In Chapter 4, we explored the relationships of *in vivo* tendon stiffness of the major lower limb tendons, using ultrasound shear wave elastography, with the metabolic energy cost of locomotion. This experimental approach was complemented by musculoskeletal simulations where tendon stiffness was varied. The experimental findings suggest lower limb tendon stiffness was not associated with whole-body metabolic power. However, the simulation results suggest correlations at the MTU-specific level may not be evident at the whole-body level. While estimating tendon stiffness with ultrasound at rest is common, it may not adequately capture MTU behavior during dynamic contractions.

The findings of this dissertation indicate MTU properties are not specialized to reduce the neuromuscular and metabolic demands of locomotion, yet these outcomes were both sensitive to optimizing individual MTU properties. Tendon stiffness uniquely affects the MTU-specific energy demands resulting in a diverse range of responses, possibly contributing to a cancelation effect at the whole-body level. Overall, our findings reinforce the difficulty of establishing a direct link between elements of the musculoskeletal system and the associated demands during locomotion.

Despite these challenges, future investigations should continue advancing our fundamental understanding of MTU function in locomotion because it holds the potential to broadly benefit many areas of human movement.

Chapter 1 – Introduction

1.1 Muscle-tendon Unit

The muscle-tendon unit (MTU) is modeled representatively as a contractile component (muscle) in series with an elastic component (tendon) [1]. The hierarchical structure of muscle consists of bundled muscle fibers composed of contractile subunits (sarcomeres), which require metabolic energy to produce force via cross-bridge cycling [2]. In contrast, tendon is composed of bundles of collagen fibers arranged in parallel, which do not directly require metabolic energy to transfer muscle force or store and release elastic strain energy. Taken together, muscle and tendon function in synchrony to produce movement.

Muscle force production depends on the amount and rate of cross-bridge formations, determined by: muscle volume, neuromuscular activation, and the force-length-velocity relationship (Figure 1A & B) [3]–[9]. These relations are key to understanding the behavior of muscle. As muscle produces force, the muscle fiber length, or muscle fascicle length, will change at a given corresponding rate [8]. Since muscle fascicles are composed of bundles of muscle fibers, the relative length change and velocity are similar in most muscles [4], [10], [11]. When the MTU contracts isometrically, muscle fibers produce force at both the optimal length and low shortening velocities (Figure 1A & B) [9], [12]–[14]. This is metabolically effective as the muscle performs little to no mechanical work, yet produces a large force with minimal neuromuscular effort given the level of neuromuscular excitation [12]–[14]. During concentric and eccentric muscle contractions, muscle fibers instead move away from the optimal length and function at higher

velocities, thus demanding increased neuromuscular effort and metabolic energy in comparison to the isometric condition (Figure 1A & B) [14]. Notably, the ascending limb of the force-length curve is mechanically stable, whereas the descending limb is generally unstable, as muscles are more susceptible to damage during eccentric contractions (Figure 1A) [15], [16]. Regardless of muscle contraction type, all muscle forces are transmitted via tendon connecting muscle to the skeletal system.

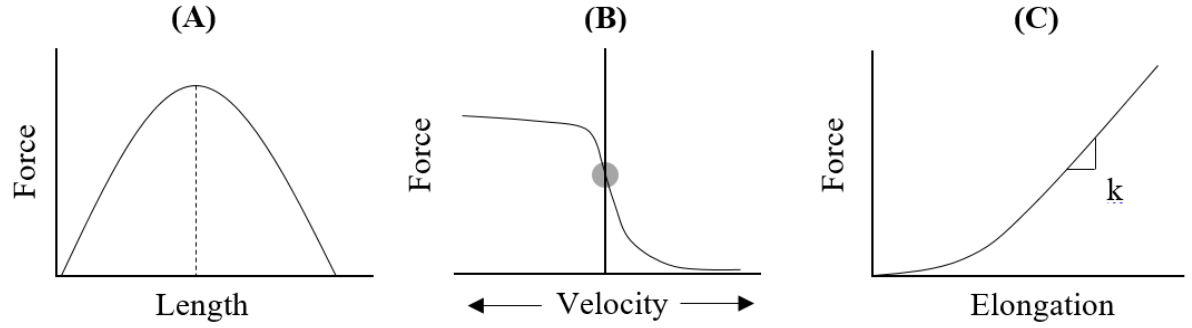

Figure 1.1 The mechanical relationships of the MTU- (A) The active force-length relationship of muscle: the dashed line represents the plateau region associated with maximum muscle force and optimal fiber length. (B) The force-velocity relationship of muscle: the shaded region where velocity equals corresponds to the maximum isometric force. (C) The force-elongation relationship of tendon- stiffness (k) can be determined from the linear region of the slope.

Though force transmission is the primary function of tendon, there is also a secondary function: storing and releasing elastic strain energy. A change in muscle fiber length and joint angle prompts tendon elongation, with greater displacements storing greater elastic strain energy, a form of potential energy [17]. Minimal muscle force is required to straighten crimped collagen fibers, resulting in an initial non-linear toe-region of the force-elongation curve (Figure 1C) [18]–[20]. This region precedes a linear elastic region as force further increases (Figure 1C) [21]–[24]. Eventually, and with excessive force, the tendon may then enter the plastic region of the force-elongation curve, where permanent deformations can lead to tendon rupture [24], [25]. Structural and material properties both determine tendon stiffness and in turn the functional mechanics of the

MTU [22], [26]. For example, tendon slack length (resting length), a structural property, is inversely related to tendon stiffness. Consequently, a tendon with excessively low stiffness can disrupt muscle force transmission, demanding increased excitation, and potentially cause limb positioning errors [5], [27], [28]. In contrast, if the tendon was absent from the MTU, or extremely rigid, the muscle fibers would inherently be forced to perform most of the mechanical work and do so at unfavorable lengths and shortening velocities, consequently decreasing the level of muscle force and elevating the metabolic energy cost of force production [28], [29]. Tendon stiffness is susceptible to changes throughout the lifetime, commonly decreasing with aging [30]–[32], injury[33], [34], and disease [35], [36], but often increasing with exercise [25], [30], [31], [37]–[40], thus impacting the metabolic energy cost of muscle contraction and movement.

A spring-like tendon provides an overall advantage to force production by decoupling the muscle fiber and tendon length changes from one another, and thus from the overall length change of the MTU [29], [41]–[45]. Muscle fibers are then permitted to perform less mechanical work and function closer to their optimal length at slower shortening velocities with less neuromuscular effort because the tendon performs the majority of the length change [45], [46]. Moreover, a spring-like tendon acts as a protective mechanism by inhibiting muscle fibers from lengthening excessively, as high forces incurred during eccentric contractions risk damaging the muscle [5], [47], [48]. Hence, muscle-tendon synergy is a critical aspect of overall MTU physiological function.

1.2 Stretch-shortening Cycles

The energy-saving mechanism of the stretch-shortening cycle occurs in ballistic human movement (walking, running, jumping, etc.) [45], [49]–[53]. The spring-like behavior of tendon

is essential to this secondary function. Upon stretching, the tendon performs mechanical work and stores elastic strain energy, which is then released upon muscle relaxation all at no additional metabolic energy cost [49], [54]. This mechanism prevents muscle from performing metabolically expensive mechanical work, in particular, positive muscle work which can demand up to fivefold more metabolic energy in comparison to negative muscle work [12], [55].

The physical properties of the MTU determine the ability to store and release elastic strain through tendon stretch and recoil; making some tendons better suited for this function than others. The long Achilles tendon connected to the short pennated fibers of the triceps surae muscle (medial and lateral gastrocnemii and the soleus muscles) is ideal for storing and releasing elastic strain energy through stretch-shortening cycles [53], [56]–[59]. This MTU structure is more common in the distal limb segments than in the proximal limb segments which are better suited for producing mechanical power [58], [60]. These ideal MTU properties also serve to reduce the volume of active muscle, thereby reducing the metabolic energy cost of muscle contraction [61].

The interaction between the triceps surae muscle and Achilles tendon reduces the metabolic energy cost of the stance phase of human locomotion, mediated by stretch-shortening cycles [49], [51], [52], [62], [63]. Achilles tendon elongation enables the triceps surae muscle fibers to operate under metabolically efficient conditions throughout the stance phase of locomotion[51], [64]. During the stance phase of walking, the triceps surae MTU is said to resemble the action of a catapult- slowly lengthening while leading up to a rapid recoil [50], [51]. In contrast, the spring-like behavior of the triceps surae during the stance phase of running is comparable to the conceptual action of a pogo stick- the loading period is nearly equal in time to the release period which lends a characteristic ‘bounce’ [17], [57], [65]. However, this behavior is spring-like merely in stretch and relaxation, not compression. Therefore, the difference in the

stretch-shortening cycle during running and walking results in divergent muscle fiber mechanics and metabolic energy cost of movement.

1.3 Locomotion

Bipedal locomotion characterizes human movement. The walking gait cycle predominantly consists of stance and swing phases, whereas the running gait cycle consists of stance and flight phases. The stance phase of walking is comparable to the motion of a simple inverted pendulum model [66], while running can be formalized as a bouncing rubber ball, or a mass bouncing on a linear spring[67]–[69]. Early studies suggested elastic strain energy was only valuable during running, but the walking gait produced by the rigid leg of the inverted pendulum model insufficiently represents the center of mass trajectory and vertical ground reaction force observed experimentally [53], [68]. This discrepancy between the conceptual model, and experimental kinematics and kinetics of walking, can be resolved using a double inverted pendulum model [70] or a spring-loaded inverted pendulum model [71]. This suggests the flexion of the knee, and possibly the storage and release of elastic strain energy within the spring-like lower limb tendons, contribute to the overall spring-like behavior of the leg during the stance phase of both walking and running [41], [71], [72].

Minimizing the metabolic energy cost of movement or neuromuscular effort are two strategies the central nervous system may adhere to during locomotion[73]–[75]. Individuals exhibiting movement disorders, such as cerebral palsy [76]–[79], or amputees [80]–[83] experience an increased metabolic energy cost of locomotion due to unfavorable kinematics and muscle mechanics. We formalize locomotor efficiency as the ratio of mechanical work and expended metabolic energy. Yet mechanical work can be calculated using a variety of methods,

potentially yielding different results [84]. For example, some biomechanists suggest walking and running efficiencies, greater than the maximum efficiency of muscle, are attainable through the 'free work' returned in stretch-shortening cycles [49], [66]. Ultimately, the behavior of the muscle fibers determines the metabolic energy cost of locomotion.

During the stance phase of walking, the medial gastrocnemius muscle fibers operate almost completely isometric and the soleus muscle fibers lengthen [41], [50], [51], [62], [63], [85]. As stance phase terminates, the ankle plantar flexes during push-off causing the gastrocnemius fascicles to operate concentrically [41], [51], [86], [87]. In contrast, throughout the stance phase of running the medial gastrocnemius muscle fibers operate concentrically and the soleus muscle fibers operate isometrically [57], [62], [63], [88]. The ankle joint contributes roughly half of the positive mechanical work during the stance phase of locomotion, and Achilles tendon elastic strain energy contributes 20-60% of the total ankle positive work [42], [89]–[91]. The Achilles tendon magnifies the work returned to the muscle as tendon can shorten faster than muscle, so nearly all of the mechanical energy stored in the tendon is subsequently returned to the muscle, suggesting minimal tendon damping [27], [46], [92]. Active MTU lengthening before muscle shortening, compared to only shortening, decreases muscle mechanical work and reduces the metabolic energy cost of locomotion [58], [93], [94]. Even though this elastic energy-saving mechanism may provide a greater advantage during running, it is still nevertheless considered beneficial during walking [23], [49], [50].

The energetic cost of human walking is relatively efficient in comparison to other species [95] and the self-selected speed, stride length, and stride frequency lower the metabolic energy cost [84], [96]–[98]. This suggests bipedalism was a strong evolutionary influence on hominid ancestors who engaged in continental migrations and persistence hunting [99]–[102]. Yet the

structure of the MTU may not have evolved to minimize locomotor economy under ideal conditions (preferred speed, level ground, etc.). During locomotion, lower limb muscles operate on all regions of the force-length curve due to the spring-like nature of tendon [86]. The lower limb MTU properties and function are well suited for locomotion in general, but the properties of the MTU are not likely optimized specifically for any given task but are rather well suited to accommodate a range of locomotive behaviors and conditions (terrain, incline, pace, etc.).

1.4 Musculoskeletal Modeling and Simulation

Musculoskeletal models are a simplified representation of the musculoskeletal system. Many musculoskeletal model measurements are derived from imaging techniques and cadaveric measurements [103]. Simulating a movement is accomplished by solving the equations of motion for a given objective criteria, and optimal control methods achieve this by optimizing (minimizing or maximizing) the movement for a given performance criteria while estimating muscle excitation patterns [104]. Minimizing muscle excitation, squared or cubed, has been shown to lead to realistic gait simulations [105]. This approach allows researchers to investigate questions that would be difficult or infeasible to accomplish in human subjects due to the invasive and ethically questionable nature of the experiments.

In a musculoskeletal model, it is possible to instantaneously alter MTU properties and observe the simulated metabolic energy cost and mechanics. Notably, muscle force is consistently most sensitive to perturbations in tendon slack length in comparison to other MTU properties (optimal muscle fiber length, physiological cross-sectional area, pennation angle, moment arm length, etc.) [106]–[109]. This is likely due to the elastic tendon ultimately influencing the muscle

contractile relationships. However, the impact of the major lower limb MTU properties on the metabolic energy cost of locomotion remains to be thoroughly explored.

An approach commonly used to characterize tendon stiffness in musculoskeletal modeling is the percent strain (relative elongation) produced at peak isometric force [110], though this varies among individuals and possibly among different MTUs [23], [46], [92], [111]–[114]. For example, the average human Achilles tendon strain at maximum isometric force typically varies among individuals, between 4 and 10% [23], [46], [92], [111], [112], [114]–[116]. This parameter can substantially impact movement performance, as well as the overall and muscle-specific metabolic energy costs, when systematically varied in the musculoskeletal model. For example, simulations of vertical jumping indicated jump height increased with a lower Achilles tendon stiffness [110]. Moreover during walking, given a 25% increase in Achilles tendon stiffness (relative to its physiological stiffness), the metabolic energy expenditure of the triceps surae muscle increased by 7%, but the overall metabolic energy cost of walking only increased by 1.5% [117]. Yet during running, the metabolic energy cost of movement was lower with a stiffer Achilles tendon [118]. This suggests tendon properties are not selectively tuned to optimize either the metabolic energy cost of walking or running. Much of the lower limb MTU properties have yet to be targeted using musculoskeletal modeling and simulation to explore the impacts of the metabolic energy cost of locomotion.

Musculoskeletal modeling and computer simulation is an insightful biomechanical research approach, but it is limited by the intense computational demand. Generating simulations of human movement can often take hours or even days to solve. With advancements in computer technology, the computational process can be sped up using parallel computing- the process of dividing the problem into smaller parts that can be solved simultaneously on computer clusters or

a multicore computer workstation [104], [119]–[124]. Exploring modern computer architecture can circumvent this limitation which has delayed the progression of musculoskeletal modeling and simulation as a more general-purpose tool for biomechanists, engineers, and clinicians.

1.5 Ultrasonography

B-model ultrasonography uses high-frequency sound waves to create real-time two-dimensional images of internal structures within the body. Images are often used to assist medical professionals with diagnosing and monitoring various medical conditions. B-mode ultrasonography can also be used to non-invasively estimate the stiffness of superficial tendons by capturing the maximum displacement of tendon during a maximum voluntary isometric contraction. This technique has been most commonly applied to the Achilles tendon due to its superficial nature and important role in walking (e.g. [23], [112], [116], [125], [126]). Subsequently, it was estimated approximately 6% of the total mechanical work involved in human walking can be attributed to the elastic strain energy stored in the Achilles tendon [23]. This technique can be physically exhausting for participants and presents several methodological challenges for the experimenter including adequate ultrasound probe placement. Moreover, these measurements can be implemented in a musculoskeletal model to characterize tendon stiffness.

More recently, ultrasound shear wave elastography (SWE) a non-invasive and reliable imaging method, has been used to estimate the elastic properties of biological soft tissues [127]. The ultrasound probe uses a non-ionizing acoustic radiation force to emit shear waves through the underlying soft tissues and measures the speed at which these waves travel [128]. The shear wave velocity (SWV) is closely related to the stiffness of tissue, with the shear waves propagating faster through stiffer tissue. Images of the tendon are acquired at rest with a freehand

approach and the ultrasound probe does not need to be secured to the participant. The experimenter can view a color map of the shear wave velocities which overlays the standard B-mode ultrasound image of the tissue of interest.

SWE is widely used to capture the stiffness in both muscle and tendon, though more commonly in muscle. Tendon is more rigid than muscle and current SWE technology has a limited ability to estimate tendon stiffness under active tension. Even under passive tension, tendon SWV is sensitive to joint positioning, though a standardized approach has not been established. Even so, SWE is commonly used to estimate the stiffness of the Achilles tendon in healthy and pathological settings (e.g. [129]–[134]). Some have also used SWE to investigate the stiffness of the patellar and quadriceps tendons (e.g. [135]–[139]), though few have investigated the other major tendons of the lower limb. Although there are mixed findings within the literature, ultrasound SWE indicates asymptomatic tendons are generally stiffer than symptomatic tendons [129], [130], [132]–[134], and physical training increases tendon stiffness [135], [136]. There is a growing interest in using SWE to measure tendon stiffness due to the non-invasive methodology and feasibility.

1.6 Justification

Lower limb MTU properties are major determinants of muscle force-length-velocity and tendon force-elongation relationships, which influence the metabolic energy cost of locomotion. This has applications ranging from enhancing our understanding of various clinical gait disorders to pushing the limits of athletic performance. It is challenging to empirically isolate and investigate changes in MTU properties in the case of disease, disuse, or in response to training. However, they are readily modifiable in a musculoskeletal model and can be isolated from other confounding

factors. Optimal control computer simulations of human locomotion can provide insight into the metabolic energy cost of movement and mechanical outcomes driven by the muscle-tendon unit properties and complement traditional human subject-centered experiments. The use of musculoskeletal modeling and computer simulation has long been limited by the substantial computational demand. However, recent algorithmic developments paired with parallel computing on multicore computers can make previously intractable problems computationally feasible. Despite considerable research, particularly on the Achilles tendon, the broad effects of lower limb muscle-tendon unit properties on the metabolic energy cost of locomotion at both the muscle-specific and whole-body levels remain poorly understood. A better understanding of muscle-tendon unit properties has broad implications for a range of prominent areas of human movement.

1.7 Aims & Hypotheses

Specific Aim 1: Identify how the number of parallel computer processor cores in a multicore workstation interacts with musculoskeletal model complexity, movement task, initial guess, and temporal mesh density to affect the runtime of human movement simulations. Musculoskeletal modeling and computer simulation allows researchers to investigate questions that would be challenging or impossible to do experimentally, but the considerable computational demand is a substantial limitation. Although we anticipated the effect on runtime and speed-up to be problem-specific, there was more focus on maximizing the current computer architecture and algorithms to facilitate the large number of simulations performed in Chapters 3 and 4

Specific Aim 2a: Identify how MTU properties affect the neuromuscular and metabolic energy demands of walking at the whole-body and muscle-specific levels. MTU properties are major

determinants of the contractile and energetic behavior of muscle. The primary MTU properties to be investigated are:

A) muscle optimal fiber length (i.e., length at which muscle fibers generate peak active force)

B) tendon slack length (i.e., longest length at which tendon produced zero force)

C) tendon stiffness (i.e., characterized as strain at maximum isometric force)

The starting points of these model parameters within the musculoskeletal model are based on averages from the literature [23], [86], [103], [116], [140].

During locomotion, the central nervous system may prioritize minimizing neuromuscular effort or the metabolic energy cost of movement, which are both insightful metrics of human performance [75]–[77]. Neuromuscular effort was defined as muscle excitation cubed and integrated over the stride and summed across muscles [105]. This quantity is thought to represent minimization of muscle fatigue and is characteristic of submaximal human movements [105], [141]. The metabolic energy cost was defined as the energy expended during walking measured by the sum of the work rate and heat rate over the stride, and neuromuscular effort was defined as muscle excitation integrated over the stride and summed across muscles [142]–[144].

Hypothesis 2a: Optimizing optimal muscle fiber lengths will permit walking with systematically lower neuromuscular effort and metabolic energy cost across muscles.

Hypothesis 2b: Optimizing tendon slack lengths will permit walking with systematically lower neuromuscular effort and metabolic energy cost across muscles.

Hypothesis 2c: Optimizing tendon stiffness will permit walking with systematically lower neuromuscular effort and metabolic energy cost across muscles.

The hypotheses imply these values are not optimal for minimizing the metabolic energy cost of walking, but rather represent tradeoffs with the need to perform other activities. For example, the starting point for the stiffness of all tendons is 4.9% at maximum isometric force; therefore, we are predicting this value represents a compromise among multiple tasks. By adjusting MTU properties on a muscle-by-muscle basis, we can achieve a lower metabolic energy cost.

Specific Aim 2b - Exploratory: Investigate how MTU properties interact with each other to affect the neuromuscular effort and metabolic energy cost of walking at the whole-body and MTU-specific levels. The specific analyses will be guided by the results obtained from Specific Aim 2a.

Specific Aim 3a: Explore the relationship of *in vivo* tendon stiffness of the major lower limb tendons on the metabolic energy cost of locomotion using ultrasound shear wave elastography. Tendons are a key element of the musculoskeletal system and are responsible for transferring the force generated by our muscles to the skeleton. The properties of tendon, such as the stiffness, influence muscle contractile mechanics which ultimately determine the metabolic energy cost of movement.

Hypothesis 3a: Lower limb tendon stiffness will affect the metabolic energy cost of locomotion in muscle-specific ways. For the Achilles tendon, it can be reasoned that greater relative stiffness will lead to a lower metabolic energy cost due to enhanced storage and release of elastic energy. However, we lack a theoretical basis or prior findings to predict the relationships for the ankle dorsiflexors and flexors and extensors of the knee.

Chapter 2 – Computational Performance of Musculoskeletal Simulation in OpenSim Moco Using Parallel Computing

2.1 Abstract

Optimal control musculoskeletal simulation is a valuable approach for studying fundamental and clinical aspects of human movement. However, the high computational demand has long presented a substantial challenge. The OpenSim Moco software package permits musculoskeletal simulation problems to be solved in parallel on multicore processors using the CasADi optimal control library, potentially reducing the computational demand. However, the computational performance of this framework has not been thoroughly examined. Thus, we aimed to investigate the computational speed-up associated with solving optimal control simulations of human movement in OpenSim Moco using multicore parallel computing. We examined the parallel speed-up for a range of musculoskeletal models and movements that included two- and three-dimensional models, tracking and predictive simulations, and walking and reaching tasks. Simulations were solved serially and in parallel using up to 18 processor cores with a variety of temporal mesh interval densities and using two different initial guess strategies. The maximum overall parallel speed-up was problem specific and ranged from 1.7 to 7.7 times faster than serial, with most of the speed-up achieved by about 6 processor cores. Parallel speed-up was generally greater on finer temporal meshes, while the initial guess strategy had a minimal impact on the speed-up. Considerable speed-up can be achieved for some musculoskeletal optimal control simulation problems in OpenSim Moco by leveraging the multicore processors often available in

modern computers. However, since the actual improvements are problem specific, achieving optimal computational performance will require some degree of exploration by the end user.

2.2 Introduction

Musculoskeletal simulation combined with optimal control techniques represents a valuable research approach capable of providing novel insights into human movement; however, computational efficiency is a major limiting factor in the widespread adoption of this technique [104], [119]. There are computationally efficient simulation techniques, such as static optimization [141], yet these algorithms are tied to a set of experimental data, do not typically include muscle-tendon dynamics, and cannot be used to predict novel movements [145]. The substantial computational cost of optimal control simulation has been reduced, in part, through algorithmic developments such as direct collocation [105], [146]–[149]. OpenSim Moco [122] is a relatively new software tool that streamlines the use of direct collocation while leveraging the user-friendly OpenSim musculoskeletal modeling environment [150]. Rapid simulation using direct collocation not only makes many computationally demanding problems tractable but can also facilitate more complex analyses such as bilevel optimization [120] and Monte Carlo methods [151], where each iteration of the algorithm involves solving a full optimal control problem.

Another way computational efficiency can be improved in optimal control simulations is by solving parts of the problem in parallel. Parallel computing is a powerful and widely applicable computational technique where components of the problem are solved simultaneously [152]. For decades, biomechanical simulations of human movement have taken advantage of parallel computing, but usually in the context of centralized high-performance computing resources (e.g., [119]) or clusters of commodity computers (e.g., [153]). Modern laptop and desktop computers

are now available with one or more processors, each containing up to dozens of processor cores. This computer architecture is ideal for OpenSim Moco, which uses the CasADi library [154] with the ability to evaluate the objective and constraint equations in parallel on multicore processors.

Although parallel computing is now possible in mainstream computers, multicore processors with more than 4-8 processor cores come at a steep financial cost. The potential for parallel computing to reduce runtime is likely to be problem-specific, depending on factors such as problem size, problem type (e.g., tracking data versus predicting movements), movement task, model complexity, and problem discretization (i.e., temporal mesh density). There is also computational overhead in parallelizing a problem, such that using more processor cores beyond a certain point may lead to no further speed-up or a reduction in computational performance. Understanding these issues allows computational scientists to select algorithms and computer architectures that best match their simulation problems given limited financial resources. Thus, the purpose of this study was to investigate how the number of processor cores used in solving optimal control musculoskeletal simulations interacts with musculoskeletal model complexity, movement task, initial guess type, and temporal mesh density to affect the simulation runtime and speed-up potential.

2.3 Methods

2.3.1 Musculoskeletal Models

Simulations of walking were generated using both two-dimensional (2-D) and three-dimensional (3-D) full-body musculoskeletal models, and simulations of reaching were generated using a 2-D upper limb model. Muscle-tendon actuators for all three musculoskeletal models were based on a Hill-type muscle model [155].

The full-body 2-D [120] and 3-D [156] musculoskeletal models were described in detail previously but will be summarized here. The 2-D sagittal plane model consisted of nine segments, 11 degrees of freedom, and 18 muscle-tendon unit actuators [155]. The foot-ground interaction was modeled using eight Hunt-Crossley contact elements under each foot [146]. The full-body 3-D musculoskeletal model consisted of 18 segments, 31 degrees of freedom, and 84 muscle-tendon unit actuators [155]. The foot-ground interaction was modeled using 11 Hunt-Crossley contact elements under each foot [157].

The upper limb musculoskeletal model was modified from the OpenSim "Arm26" model [158], which was based on a previously published 3-D model [159]. The original planar Arm26 model [158] consisted of three segments, two degrees of freedom, and six muscle-tendon actuators. We extended the Arm26 model by adding six additional muscles from [159] to provide more robust control of the glenohumeral joint. The muscles added to the model were: anterior deltoid (DELT1), posterior deltoid (DELT2), teres major (TMAJ), pectoralis major (PECM), latissimus dorsi (LAT), and coracobrachialis (CORB).

2.3.2 Simulations

All simulations were run serially and in parallel across a range of processor cores (1, 3, 6, 9, 12, 15, and 18). 2-D tracking simulations, 2-D predictive simulations, and 3-D tracking simulations of a step of walking (1.3 m/s) were generated using OpenSim Moco 4.3 [122] and MATLAB 2020a (Mathworks, Natick, USA) on a multicore computer workstation (Intel(R) Core(TM) i9-7980XE CPU @ 2.6 GHz, 18-core processor, and 64 GB of RAM). To generate the simulation, OpenSim Moco relies on the CasADi library [154], which provides a framework for

solving numerical optimal control problems, and the IPOPT optimizer [160], which solves the nonlinear program (NLP) using a gradient-based approach.

The tracking objective function was a weighted sum of the tracking error (i.e., squared deviation of the simulation from experimental kinematic and ground reaction force data) and the sum of squared muscle excitations [161]. The predictive objective function was the sum of cubed muscle excitations [105]. The walking step duration (0.54 s) was divided into n temporal mesh intervals, resulting in 2n+1 collocation nodes using a Hermite-Simpson discretization scheme [122]. The problems were solved over a range of mesh interval densities (5, 25, 50, and 100). The finest mesh density used for the 3-D simulations was 75 rather than 100, due to inconsistent convergence at 100 mesh intervals. The optimal control problems were each solved twice using two different types of initial guesses: a dynamically consistent guess (CG) in which the model was already stepping, but was not close to the final solution, and a mesh refinement (MR) strategy, whereby the solution at a particular mesh density (e.g., 5) was used as the initial guess for the next greater mesh density (e.g., 25) [147]. For the CG case, the same initial guess was used for every mesh interval density.

Predictive simulations of discrete point-to-point forward reaching were solved using the same computer as for the walking simulations. The desired motion began with the arm down at the side of the torso with the elbow slightly flexed (shoulder elevated 0°, elbow flexed 20°) and the final target position had the arm projected in front of the torso with the elbow likewise slightly flexed (shoulder elevated 75°, elbow flexed 20°). The joint angular velocities for the initial and final positions were both zero. The objective function for the reaching task was to complete the motion in the minimum amount of time. A range of mesh interval densities (10, 25, 50, 100) was selected to solve the problem. The reaching simulations would not converge on the coarsest mesh

interval used in the simulations of walking (5 intervals); thus, the coarsest mesh interval density was set to 10 for reaching. As with the walking simulations, the optimal control reaching problem was solved twice for each mesh density using CG and MR initial guesses. The CG strategy for the reaching simulations began with an initial guess in which the model was already moving, but was not close to the final solution.

Computers with multicore processors provide the opportunity not only to solve a single problem in parallel but also to solve multiple problems simultaneously. Based on the initial results obtained in this study, we conducted a secondary analysis of the overall speed-up associated with generating multiple simulations simultaneously using the parallel for loop (parfor) included in the MATLAB Parallel Computing Toolbox. As an exemplar case for this secondary analysis, we solved 2-D predictive simulations of walking on a 50 mesh time interval using six processor cores with a CG. The runtime required to generate three simulations sequentially was compared with the runtime required to generate the three simulations simultaneously within a parfor loop.

2.3.3 Evaluation

Each simulation was run three times across the range of processor cores, temporal mesh densities, and initial guess types. Solving the same problem repeatedly leads to the same result; however, the runtime can vary slightly. Therefore, computational runtimes were averaged across the three independent runs for each case. The speed-up using parallel computing in comparison to the serial case was quantified as (Eq. 1).

$$\text{speed-up} = \frac{\text{serial runtime}}{n \text{ parallel runtime}} \quad (1)$$

where n is the number of processor cores used in parallel. The overall runtimes accounted for time spent in the IPOPT algorithm (e.g., determining the Newton step, solving linear systems) and the time spent

evaluating the NLP functions (e.g., objective function, objective gradient, constraints Jacobian). For the OpenSim Moco end user, the NLP function evaluations can be easily parallelized across multiple processor cores by setting a single CasADi parameter. The solution of the sparse linear systems encountered in the IPOPT algorithm can also be parallelized, in principle, but in practice this is more complicated for the end user and depends on the particular linear solver being used (several are available) and the linear algebra subroutines the solver was compiled against. In this study, we only evaluated parallelization of the NLP function evaluations. The proportion of total runtime that is spent evaluating the NLP functions can vary among problems; therefore, so does the speed-up potential in our approach. Thus, in addition to reporting the overall speed-up, we also examined the speed-up of just the part representing the NLP function evaluation to understand how the parallelized part of the problem scales within the problem.

2.4 Results

The runtimes for 2-D tracking simulations of walking ranged between 1.3 minutes and 3.4 hours across the tested mesh interval densities, number of computer processor cores, and initial guess strategies (Figure 2.1 A & B). Both initial guess strategies resulted in a similar overall runtime, however, the runtimes for simulations using an MR strategy were slightly greater than the runtimes for simulations using a CG strategy on mesh intervals densities of size 25 and 100, but not 50 (Figure 2.1 A & B). The overall speed-up due to parallelization for the 2-D tracking simulations of walking was minimal. The greatest speed-up using either initial guess strategy was only about 1.7 times faster than serial, with most of the speed-up achieved by about 6 processor cores regardless of the initial guess strategy (Figure 2.2 A & B).

2-D predictive simulations of walking had runtimes between 54.9 seconds and 33.6 minutes depending on the mesh interval density, number of computer processor cores, and initial guess strategy (Figure 2.1 C & D). Both initial guess strategies resulted in similar overall runtimes,

but the runtimes for simulations using a CG were slightly greater than the runtimes for simulations using an MR strategy on mesh intervals densities of size 5, 50, and 100, but not 25 (Figure 2.1 C & D). The maximum speed-up varied from about 3.7-3.8, depending on the initial guess strategy, with most of the speed-up achieved by 6 processor cores (Figure 2.2 C & D).

3-D tracking simulations of walking had runtimes between 2 hours and 53 hours (Figure 2.1 E & F). Similar to 2-D predictive simulations of walking, the runtimes for simulations using a CG were consistently greater than the runtimes for simulations using an MR strategy on mesh intervals densities of size 50 and 75, but not 25 (Figure 2.1 E & F). Runtimes between the two initial guess strategies for the 3-D tracking simulations differed the most, with simulations using a CG strategy completing 2.3 times slower overall than simulations using an MR strategy (Figure 2.1 E & F). The maximum speed-up factor for 3-D tracking simulations of walking using a CG strategy was 4.1 times faster than serial, and 3.5 times faster than serial when using an MR strategy, with most of the speed-up achieved by 6-9 processor cores (Figure 2.2 E & F).

2-D predictive simulations of reaching had runtimes between 1.3 minutes and 1.2 hours. Reaching simulations using a CG strategy were 2.1 times slower overall than simulations using an MR strategy (Figure 2.1 G & H). The runtimes using a CG strategy were consistently greater than the runtimes for simulations using an MR strategy on mesh intervals densities of size 5, 25, and 100, but not 50 (Figure 1 G & H). 2-D predictive simulations of reaching achieved the greatest speed-up ranging from 7.5-7.7 times faster than serial, depending on the initial guess strategy (Figure 2.2 G & H). The potential for further speed-up beyond 9 cores depended on the temporal mesh density (Figure 2.2 G & H). 2-D predictive simulations of reaching benefitted the most from parallelization. There was a general increase in speed-up factor when using finer mesh interval densities and more processor cores, regardless of the initial guess strategy (Figure 2.2 G & H).

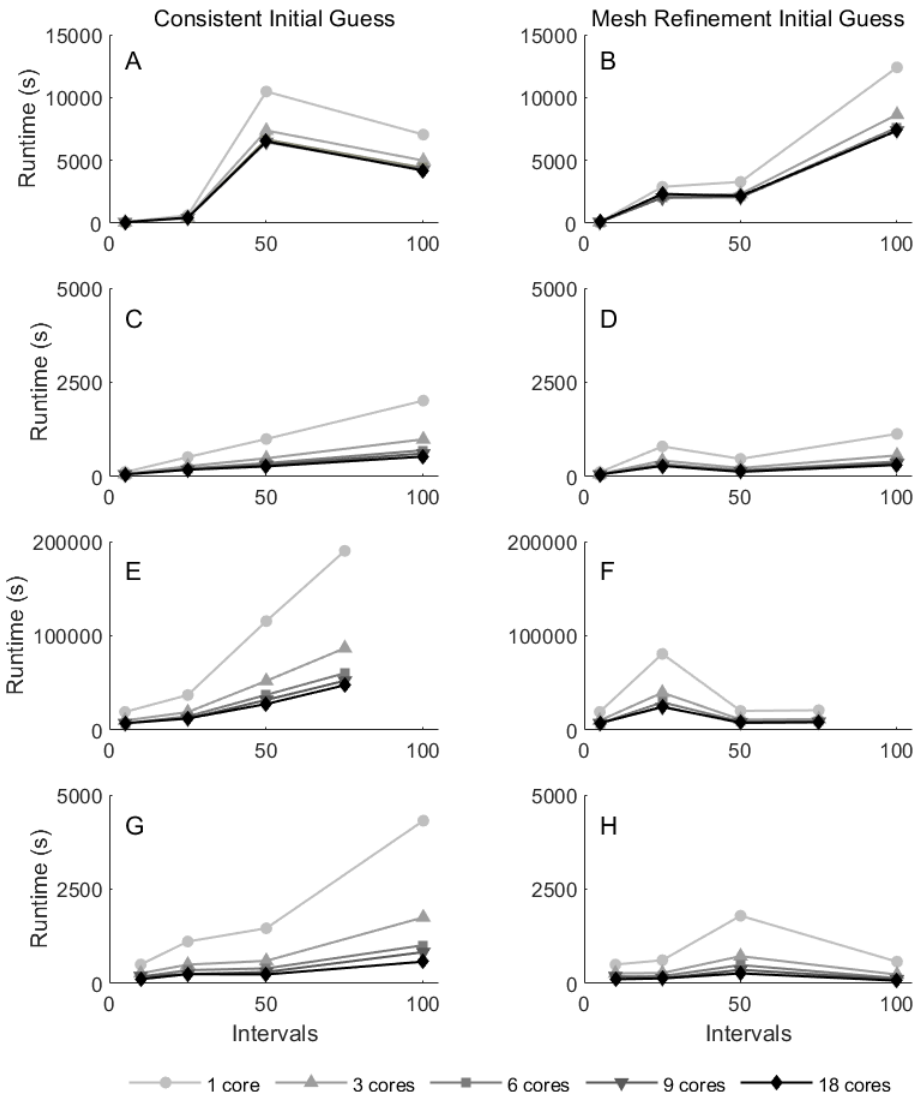

Figure 2.1 The computational runtime for 2-D tracking simulations of walking (A & B), 2-D predictive simulations of walking (C & D), 3-D tracking simulations of walking (E & F), and 2-D predictive simulations of reaching (G & H) across a range of computer processor cores and mesh interval densities. Note the different vertical ranges among the different rows of plots.

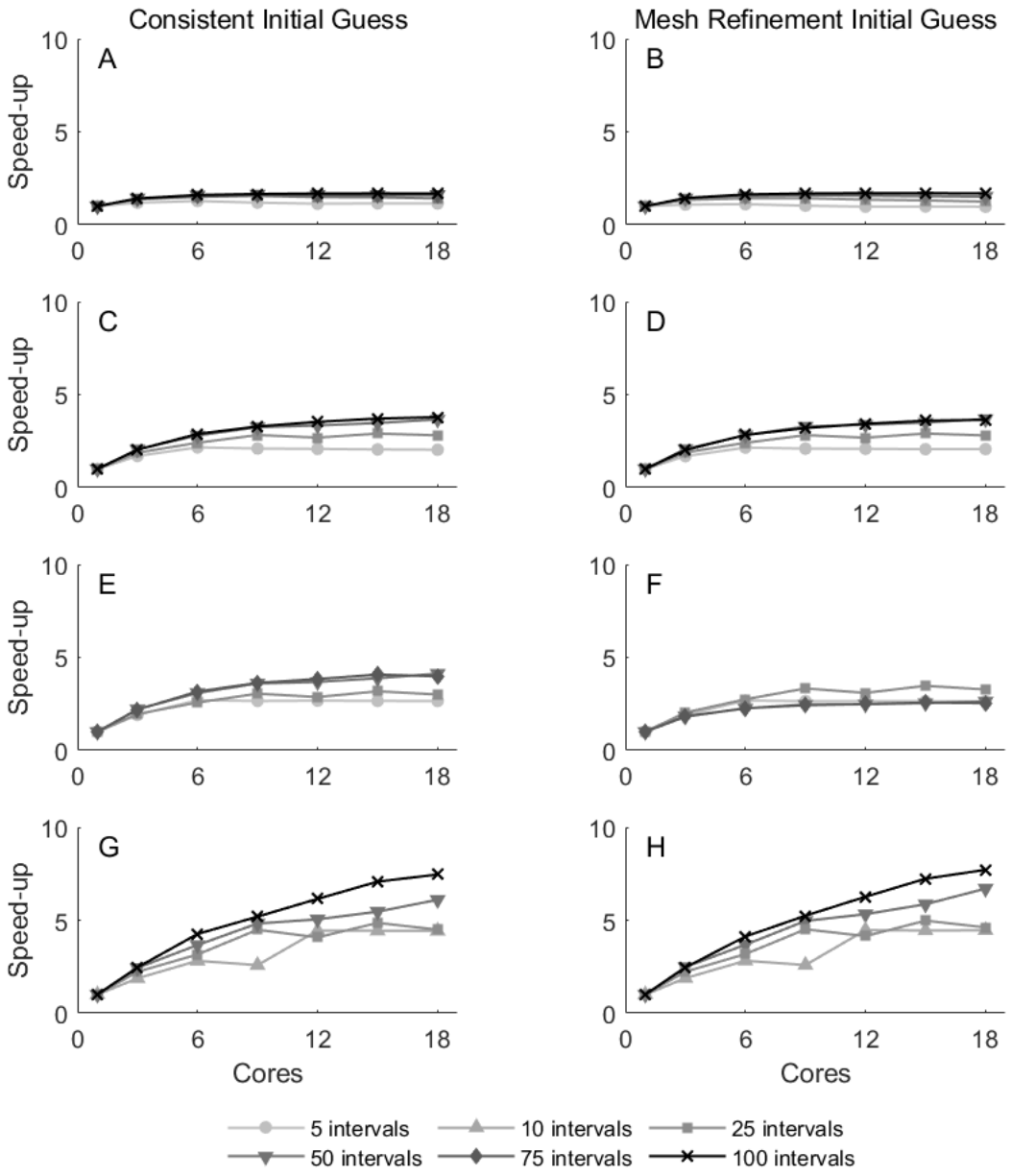

Figure 2.2 The overall computational speed-up factor for 2-D tracking simulations of walking (A & B), 2-D predictive simulations of walking (C & D), 3-D tracking simulations of walking (E & F), and 2-D predictive simulations of reaching (G & H) across a range of computer processor cores and mesh interval densities. The maximum speed-up factor varied from about 1.7 to 7.7 across the different simulations, being greatest for the 2-D simulations of reaching, and lowest for the 2-D tracking simulations of walking.

Only parallelization of the NLP function evaluation of each simulation was evaluated in this study. The speed-up for the NLP function evaluations generally increased with mesh interval density and the number of processor cores (Figure 2.3). The speed-up for the NLP function evaluations (Figure 2.3) was greater than the overall speed-up (Figure 2.2) for 2-D tracking simulations of walking, 2-D predictive simulations of walking, and 3-D tracking simulations of walking. The speed-up for the NLP function evaluations (Figure 2.3) was similar to the overall speed-up (Figure 2.2) for 2-D predictive simulations of reaching.

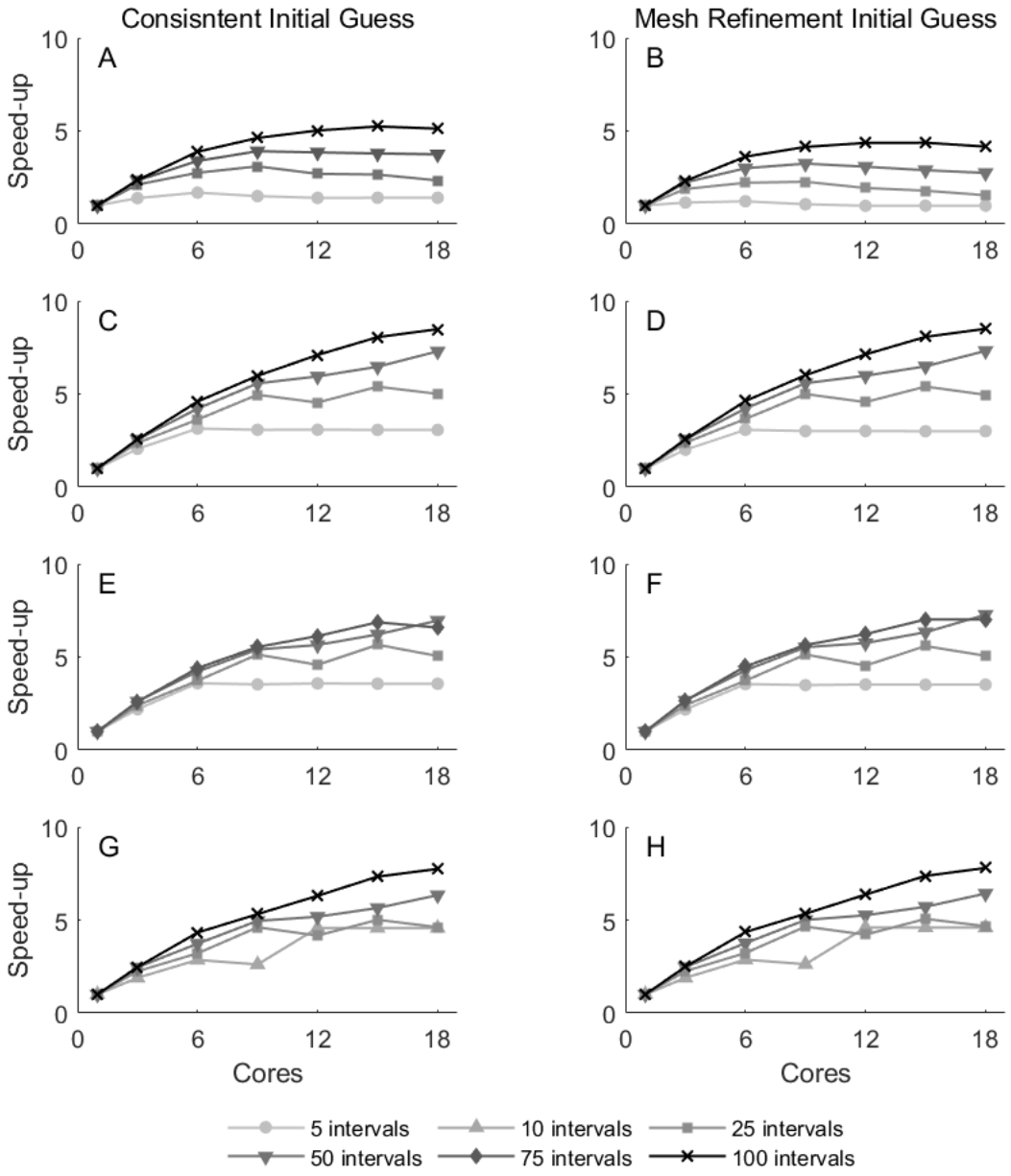

Figure 2.3 The computational speed-up factor of the nonlinear programming (NLP) function evaluation of the optimal control problem for 2-D tracking simulations of walking (A & B), 2-D predictive simulations of walking (C & D), 3-D tracking simulations of walking (E & F), and 2-D predictive simulations of reaching (G & H) across a range of computer processor cores and mesh interval densities. The maximum speed-up factor varied from about 4.4 to 8.5 across the different simulations, being greatest for the 2-D predictive simulation of walking, and lowest for the 2-D tracking simulations of walking.

The percent of overall runtime spent on NLP function evaluations ranged from 35.8% for 2-D tracking simulations to 95.6% for 2-D predictive simulations of reaching (Table 2.1). The percent of overall runtime spent on NLP function evaluations for the 2-D predictive simulations of walking and 3-D tracking simulations of walking were similar to each other, at slightly more than half of the total runtime (Table 2.1).

Table 2.1 Mean percentage of total runtime spent on nonlinear programming (NLP) function evaluations in solving the optimal control problems (± 1 standard deviation).

Simulation type	Time spent on the NLP function evaluations (%)
2-D tracking walking	35.8 ± 12.8
2-D predictive walking	54.3 ± 13.4
3-D tracking walking	58.6 ± 17.1
2-D predictive reaching	95.6 ± 2.1

Note: Data were averaged for each model and task across the number of processor cores, mesh intervals, and initial guess types.

For both 2-D and 3-D tracking simulations of walking, the minimum objective function values were greatest on the coarsest mesh density, and fairly consistent for finer meshes (Figure 2.4 A & C). For 2-D predictive walking and reaching simulations, the minimum objective function values were consistent across all mesh interval densities (Figure 2.4 B & D). The initial guess strategy had little effect on the minimum objective function values (Figure 2.4).

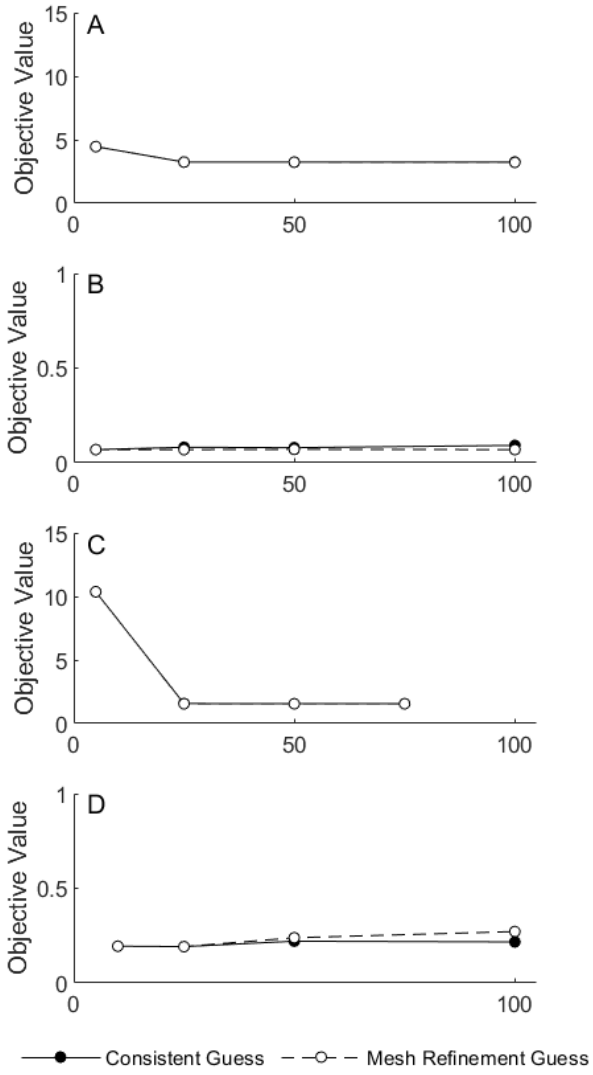

Figure 2.4 The minimum objective function values for 2-D tracking simulations of walking (A), 2-D predictive simulations of walking (B), 3-D tracking simulations of walking (C), and 2-D predictive simulations of reaching (D) across a range of mesh interval densities using both initial guess strategies. For some problems (B & D), the minimum objective function value was consistent across mesh interval densities, while for other cases (A & C) the minimum objective function value was greater on coarse meshes. The initial guess strategies had little impact on the minimum objective function value across mesh densities. Note the different ranges on the vertical axes among panels.

The iteration count ranged from 21-1084 across the different simulations and initial guess strategies. There were no consistent trends in the number of iterations required to solve the four

optimal control problems for either initial guess strategy across mesh interval densities (Figure 2.5). The MR strategy allowed 3-D tracking simulations of walking and 2-D predictive simulations of reaching to converge to a solution in considerably fewer iterations on finer mesh densities (Figure 5 C & D**)**. Yet, this was not true for the other problems, especially in 2-D tracking simulations of walking (Figure 5A).

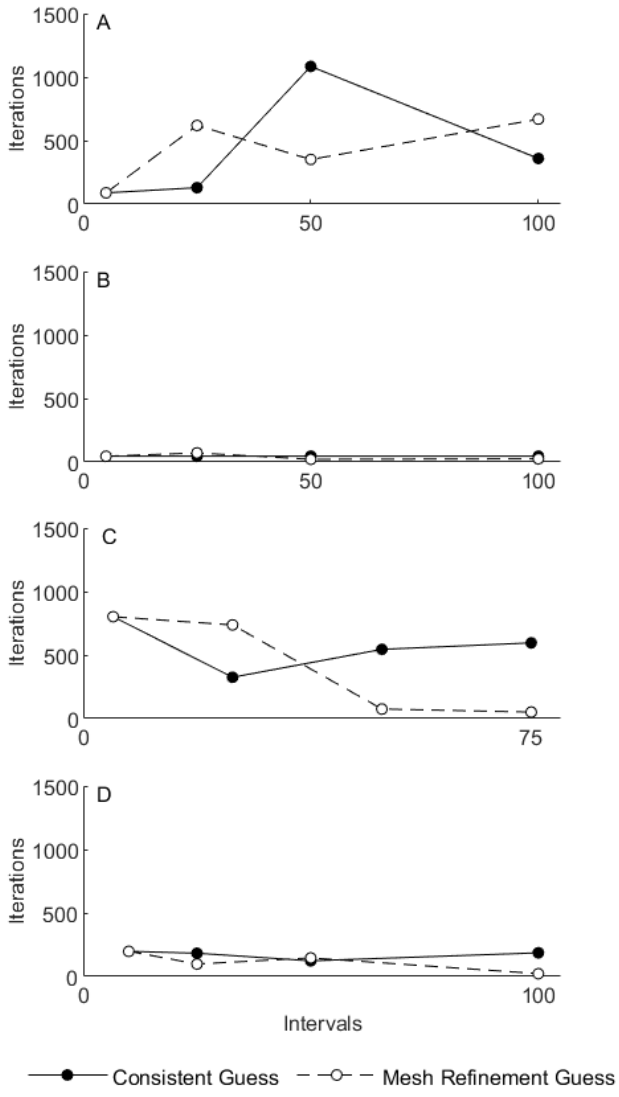

Figure 2.5 The iteration count for 2-D tracking simulations of walking (A), 2-D predictive simulations of walking (B), 3-D tracking simulations of walking (C), and 2-D predictive simulations of reaching (D) across a range of mesh interval densities using both initial guess strategies. The number of mesh intervals and initial guess strategy did not have consistent effects on the number of iterations needed to converge to a solution across conditions.

The cumulative runtime to solve the 2-D predictive walking simulation (50 mesh time interval, six processor cores, CG) three times consecutively was 17.8 minutes. The runtime to solve the same three problems within a parallel for loop was 6.1 minutes. Thus, given the 18 available processor cores in this study, it was possible to achieve an overall 2.9 speed-up factor beyond that obtained by parallelizing the NLP function evaluations within the individual simulations. Solving the same 2-D predictive walking problem three times consecutively in the serial case resulted in a cumulative runtime of 49.9 minutes. Thus, combining parallelization of the NLP function evaluations and parallel solution of the individual simulations results in an overall 8.2 speed-up factor.

2.5 Discussion

In the present study, we evaluated how model complexity, movement task, initial guess type, and temporal mesh density affect the speed-up of optimal control simulations of human movement when parallelized across a range of computer processor cores in a single computer workstation. Parallel computing has been used in biomechanics research for decades on supercomputers and computer clusters [119], [153] but can now be implemented on a typical laptop or desktop computer. The optimal control algorithms [154] implemented in OpenSim Moco [122] are well-suited for a computer with a multicore processor with the potential to improve computational performance. For all of the simulations considered here, multicore parallel computing resulted in at least some improvement in computational performance, but the extent of the speed-up varied considerably across the different simulations.

The overall degree of speed-up was closely related to the percent of total runtime spent evaluating the NLP function evaluations. That portion of the total runtime was greatest for the 2-

D predictive simulations of reaching and was lowest for the 2-D tracking simulations of walking (Table 2.1), which respectively had the greatest and least effective parallel speed-up (Figure 2.2). The 2-D predictive walking and 3-D tracking walking problems differed in problem size and type, yet had similar percentages of the total runtime represented by the NLP function evaluations (Table 2.1), resulting in similar overall parallel speed-up (Figure 2.2). Thus, while the overall speed-up achieved with multicore parallel processing in OpenSim Moco is problem-specific, it appears to be well predicted by the split between the time spent in the IPOPT algorithm versus the time spent evaluating the NLP function evaluations, which can be readily determined for any particular problem.

In most cases, the overall speed-up was greatest between 3-6 processor cores, with most of the improvement achieved by 3 processor cores. Only for the reaching simulations on finer meshes was there considerable speed-up beyond 6 cores, albeit still less than ideal linear speed-up. Therefore, most of the achievable speed-up for the simulations considered here can be realized on computers with only 4 processor cores, which is common in modern computers. The availability of more processor cores, which comes at a financial cost, can yield additional speed-up for certain problems, such as the upper limb reaching task, or by allowing multiple problems to be solved simultaneously on the same computer. We used a parallel for loop to solve multiple problems in parallel, as might be typical in a Monte Carlo simulation or bilevel optimization, but it would also be possible to start multiple unrelated instances of OpenSim Moco simultaneously. The main consideration in either case is deciding how to allocate the available processor cores within and between the multiple OpenSim Moco problems that are being solved in parallel.

The maximum possible overall speed-up in this study was limited by the fact that we only investigated parallelization of the NLP function evaluations. That was our focus because the

CasADi library [154] used in OpenSim Moco [122] makes it easy to select the number of parallel threads used for that part of the problem. Thus, parallelizing the NLP function evaluations is likely to be representative of typical user behavior. A systematic investigation of parallelization within the linear equation solvers available in IPOPT (e.g., [162]) could potentially lead to further enhancements in computational performance and should be a focus for future research. Even within the part of a problem that is parallelized there are likely to be differences in the actual speed-up that is realized. Thus, we evaluated the speed-up achieved in the NLP function evaluations, separate from the overall speed-up. Speed-up is considered "ideal" when doubling the number of processor cores doubles the computational speed. For most problems, the speed-up for the NLP function evaluations was substantially greater than the overall speed-up. However, even in the best case (2-D predictive walking, Figure 2.3 C) the speed-up was less than ideal. Near ideal speed-up was previously reported for evaluating the objective and constraints derivatives in the solution of a direct shooting problem of human walking on a distributed memory parallel supercomputer [119]. The discrepancies from the present results are likely due to different optimal control formulations (direct shooting versus direct collocation in the present study) and different computer architectures (independent compute nodes versus a single multicore processor in the present study).

The individual runtimes varied considerably across models and tasks, number of mesh intervals and processor cores, and initial guess types (Figure 2.1). However, our primary focus was not the runtimes per se, but rather the speed-up obtained through parallel computing. In contrast to the runtimes, the speed-up that was achieved generally scaled consistently across mesh intervals and processor cores, and was similar for the two different initial guess types (Figure 2 & 3). Generating simulations of human movement using direct collocation involves discretizing the

problem over a temporal mesh. Using a coarse mesh will usually reduce computation time, but could impair the quality of the solution. Solving a problem on a finer mesh may lead to a higher quality solution, but at the cost of being more computationally intensive [149]. In the current study, solutions obtained on finer mesh interval densities generally resulted in a greater speed-up when parallelized across more processor cores than solutions obtained on coarser mesh interval densities. Thus, the computational efficiency achieved through parallel computing helped offset the computational demands of using finer temporal mesh densities.

This study had several limitations. Parallelizing only the NLP function evaluation part of the problem limited the overall speed-up that was possible. However, it is important to note this approach likely reflects how a typical OpenSim Moco user would parallelize optimal control simulations of human movement. Additionally, the walking and reaching tasks that we used are common in the literature, yet there are many other tasks that have also been simulated using musculoskeletal models. The present results will not necessarily generalize to simulations of other tasks. Finally, OpenSim Moco can solve problems that we did not consider here, such as determining the muscle states that correspond to a prescribed motion (i.e., a Moco Inverse problem). The potential for parallel computing to speed-up these other problem types cannot be inferred from the present results. We chose to focus on tracking and predictive optimal control problems as they tend to be the most computationally demanding.

Herein, we analyzed the computational demands of a broad range of optimal control simulations of human movement using parallel computing in OpenSim Moco. While the speed-up achieved was not ideal, the computational performance improved for all of the examined simulations when solved in parallel, and solving multiple problems simultaneously yielded further computational speed-up. In summary, multicore parallel computing in OpenSim Moco via the

CasADi library provides an effective means to reduce the computation demand of optimal control musculoskeletal simulation, enhancing the feasibility of this research technique.

Chapter 3 – Optimized Muscle-Tendon Unit Properties for Human Walking

3.1 Abstract

The muscle-tendon unit (MTU) is a complex biomechanical system responsible for generating and transmitting forces to produce movement. The structural features of the MTU, such as optimal muscle fiber length, tendon slack length, and tendon stiffness, are major determinants of the overall contractile behavior of muscle and the metabolic energy cost of movement. The impact of individual features of MTU on whole-body musculoskeletal function is poorly understood but is central to our fundamental understanding of movement biomechanics. Therefore, the purpose of this study was to identify how MTU properties affect the neuromuscular and metabolic energy demands of walking at the whole-body and muscle-specific levels. We used a bilevel optimization technique with modeling and simulation to investigate the effects of lower limb optimal muscle fiber length, tendon slack length, and tendon stiffness on the neuromuscular and metabolic demands of human walking. The simulation objective function was specifically defined to minimize neuromuscular effort. Whole-body neuromuscular effort was 16.6-67.6% lower while whole-body metabolic power was 0.2-9.5% lower during walking compared to the default parameter values. Simultaneously optimizing optimal muscle fiber length and tendon slack length produced the lowest neuromuscular effort, and optimizing tendon slack length alone produced the lowest metabolic cost. Despite reductions in whole-body neuromuscular and metabolic energy demands, the demands of each MTU were different and not all lower than the default parameter values. MTUs are not specifically tuned to minimize the demands of normal

speed level walking and can be optimized to lower neuromuscular effort and metabolic energy cost. An evolutionary trade-off may exist between the need to perform other tasks besides level walking at the preferred speed and the biological MTU features.

3.2 Introduction

The interaction of muscle and tendon is important for human movement and the properties of each component can uniquely affect the associated neuromuscular and metabolic demands. Optimal muscle fiber length (OFL) is a key feature of the muscle-tendon unit (MTU), and the force-length-velocity relationship is a major determinant of the overall contractile behavior of muscle. When muscle fibers operate at the OFL, force is generated with less neuromuscular effort, or neuromuscular excitation, and less metabolic energy due to optimal cross-bridge formations [2], [6], [8]. Minimizing neuromuscular effort or metabolic energy cost, which often coincide with each other, is indicative of preferred gait characteristics [73]–[75]. Additionally, spring-like tendons not only transfer muscle force to the skeletal system to produce movement, but tendon stiffness (TK) affects where the muscle fibers operate along the force-length-velocity curve [28], [29]. A spring-like tendon can lower the metabolic energy cost of force production by reducing expensive metabolic changes in muscle mechanical work [29], [41]–[45]. While muscle and tendon functions are complementary to each other, the properties of each may not be tuned to minimize the demands of walking. Bipedal walking is important to human behavior and was likely influential in the development of our musculoskeletal evolution [163], [164]. Even so, the neuromuscular activation of individual MTUs is not uniformly tuned for a specific type of locomotion or speed [165].

The properties of both muscle and tendon are contributing factors affecting the metabolic energy cost of locomotion, however, these contributions are difficult to generalize due to the natural variety of anatomical shapes and locomotor functions among human lower limb MTUs. The impacts of individual MTU properties on the function and metabolic energy cost of the whole-body musculoskeletal system are poorly understood but of considerable interest to better understand the fundamental biomechanics of human locomotion.

Relative muscle fiber lengths and tendon slack lengths (TSLs) vary considerably across species and are likely subject to selective pressures. For example, the ratio of TSL to OFL is greater in humans than in our closest extant relatives, chimpanzees [86], [166]. This implies there are differences in lower limb MTU properties possibly driven by the functional demands of bipedal locomotion. Additionally, the substantial anatomical variation among the lower limb MTUs can impact the mechanical function, and thus the metabolic energy cost of force production. Furthermore, muscle fiber lengths, both absolute and relative to limb length, can change over time due to exercise [167]–[170] and aging [171]–[173]. Experimental approaches to studying the effects of MTU properties in humans are limited to cross-sectional studies and time-consuming longitudinal interventions. Musculoskeletal modeling and simulation is a complementary approach that allows muscle parameters to be varied systematically, or optimized for various performance criteria.

The triceps surae is often the focus when studying the effects of muscles, tendons, and their interaction on MTU mechanics during locomotion due to its superficial nature and essential role in locomotion. While the ankle extensors play an important role in supporting and propelling the body in locomotion, their energy consumption is estimated to represent only 25% of the net metabolic cost of walking [143]. Compared with the triceps surae, the effects of OFL, TSL, and

TK across other major lower limb muscles on the neuromuscular effort and metabolic energy cost of walking are largely unknown at the whole-body and MTU-specific levels.

In this study, we used a modeling and simulation approach to determine how OFL, TSL, and TK affect the neuromuscular effort and metabolic energy cost of walking. Neuromuscular effort was defined as muscle excitation cubed and integrated over the stride and summed across muscles [105]. This quantity is thought to represent minimization of muscle fatigue and is characteristic of submaximal human movements [105], [141]. Likewise, metabolic energy cost was defined as the energy expended during walking quantified as muscle heat rate plus muscle work rate, integrated over the stride and summed across muscles [142]–[144]. We hypothesized optimizing the MTU properties in the lower limb MTUs would permit walking with lower neuromuscular effort and metabolic energy cost across muscles.

3.3 Methods

Three musculoskeletal model parameters: OFL, TSL, and TK were separately optimized in the lower limb MTUs during simulations of human walking. In a secondary analysis, we simultaneously optimized OFL and TSL in the lower limb MTUs to better investigate the muscle-tendon interaction. We used a bilevel optimization technique where the upper level of the problem was solved with a genetic algorithm to search for the optimal OFL, TSL, and TK MTU parameters. The process of the genetic algorithm is inspired by natural selection observed in evolutionary biology [174]. The genetic algorithm function evaluations were evaluated using parallel computing through the MATLAB Parallel Computing Toolbox. The lower level solved an optimal control simulation of human walking using OpenSim Moco [122] using the MTU parameter values determined using the genetic algorithms.

3.3.1 Musculoskeletal Model

A two-dimensional musculoskeletal model developed by Nguyen et al., 2019 [120] was used to simulate human walking. The model is summarized here and is described in more detail in Appendix A. The sagittal plane model consisted of nine segments, 11 degrees of freedom, and 18 muscle-tendon unit actuators [155]. The foot-ground interaction was modeled using eight Hunt-Crossley contact elements under each foot [146].

OFL, TSL, and TK were individually optimized for all lower limb MTUs using the genetic algorithm in the upper level of the optimization. The size of each parameter's search space was expanded beyond the default parameter values based on the computational feasibility and was unique for each MTU parameter (Table 3.1). TK was characterized as tendon strain produced at maximum isometric force (F_{max}). A low tendon strain at F_{max} represents a stiffer tendon, with 0% tendon strain at F_{max} representing a perfectly rigid tendon.

3.3.2 Simulations

Predictive simulations of a step of walking at 1.3 m/s (step time 0.54 s) were generated using direct collocation with a grid density of 15 nodes using OpenSim Moco 4.4 [122] and MATLAB (2022a, MathWorks, Natick, MA, USA). The optimal control problem was set to minimize the sum of cubed muscle excitations (referred to here as neuromuscular effort), which has been shown to lead to realistic gait simulations [105]. Simulations were generated on a multicore computer workstation (Intel® Core™ i9-7980XE CPU @ 2.6 GHz, 18-core processor, and 64 GB of RAM).

The genetic algorithm optimized nine variables (one for each unique MTU in the musculoskeletal model). The population size was set to 108 as this was determined to be

sufficiently large enough for the current problem and maximized the computation power of our computational workstation. The bilevel optimization terminated after 50 generations because during pilot testing we found no meaningful reduction in the objection function value beyond this point. The solution of the populations in the genetic algorithm was parallelized across the 18 processor cores because this was found to achieve better computational efficiency than parallelizing the individual optimal control problems that were solved in the lower level of the bilevel problem.

Based on the initial results obtained in the current study, we conducted a secondary analysis where OFL and TSL were simultaneously optimized. Solving optimal control musculoskeletal simulations has a high computational demand. Embedding this technique in a bilevel optimization further increased the size and complexity of the problem, and thus the computation demand. We found that it was too computationally demanding and complex to simultaneously optimize OFL, TSL, and TK across all major lower limb MTUs. Among the possible parameter combinations, we chose to optimize OFL and TSL simultaneously because these parameters had the greatest change in neuromuscular effort and metabolic energy cost.

3.3.3 Evaluation

The musculoskeletal model parameters were optimized three separate times starting from different random points in the solution space, and the MTU parameters producing the simulation with the lowest objective function value were further analyzed. The optimal gait simulations were used to estimate neuromuscular effort and metabolic energy cost at the whole-body and MTU-specific levels [144]. Neuromuscular effort and metabolic energy cost were further evaluated across the major muscle groups of the lower limb: hip extensors (HE), knee extensors (KE), ankle

extensors (AE), and flexors (FX) [143]. The HE group included the hamstrings and gluteus maximum, the KE group included the rectus femoris and vasti, the AE group included the gastrocnemius and soleus, and the FX group included the iliopsoas, biceps femoris short head, and dorsiflexors [124]. The FX group represented a collection of muscles responsible for flexing the joints of the lower limb, rather than a joint-specific grouping.

3.4 Results

The individually optimized MTU parameter values were all at least somewhat different from the default parameter values. (Figure 3.1). MTU-specific changes in parameter values were generally different across MTUs, with some consistencies among muscle groups. OFL became longer in the KE group but shorter in the AE group (Figure 3.1 A & B). TSL became longer in the HE group but shorter in the AE and FX groups (Figure 3.1 C & D). TK became less stiff in the KE group, but there was no uniform increase in TK among muscle groups (Figure 3.1 E & F). There were no discernable patterns within the uniarticular muscles or biarticular muscles.

Table 3.1 The default musculoskeletal model parameter values (P_0) for optimal muscle fiber length (OFL), tendon slack length (TSL), and tendon stiffness (TK). TK was characterized as tendon strain produced at maximum isometric force (F_{max}). A low tendon strain at F_{max} represents a stiffer tendon, with 0% tendon strain at F_{max} representing a perfectly rigid tendon. The lower bound (LB) and upper bound (UB) are the limits of the parameter search space (OFL= P_0±25%, TSL= P_0±5%, and TK= P_0±50%). The represented muscle-tendon units include: hamstrings (HAM), biceps femoris short head (BFsh), gluteus maximus (GMAX), iliopsoas (IL), rectus femoris (RF), vasti (VAS), gastrocnemius (GAS), soleus (SOL), dorsiflexors (DOR).

	OFL (m)			TSL (m)			TK (% strain at F_{max})		
Muscle	LB	P_0	UB	LB	P_0	UB	LB	P_0	UB
HAM	0.09	0.12	0.15	0.26	0.35	0.44	0.04	0.05	0.06
BFsh	0.08	0.11	0.14	0.12	0.16	0.20	0.04	0.05	0.06
GMAX	0.12	0.16	0.20	0.06	0.08	0.10	0.04	0.05	0.06
IL	0.08	0.11	0.14	0.11	0.15	0.19	0.04	0.05	0.06
RF	0.06	0.08	0.10	0.29	0.39	0.49	0.04	0.05	0.06
VAS	0.09	0.12	0.15	0.11	0.14	0.18	0.04	0.05	0.06
GAS	0.05	0.06	0.08	0.30	0.40	0.50	0.04	0.05	0.06
SOL	0.03	0.04	0.05	0.20	0.27	0.34	0.04	0.05	0.06
DOR	0.05	0.07	0.09	0.20	0.26	0.33	0.04	0.05	0.06

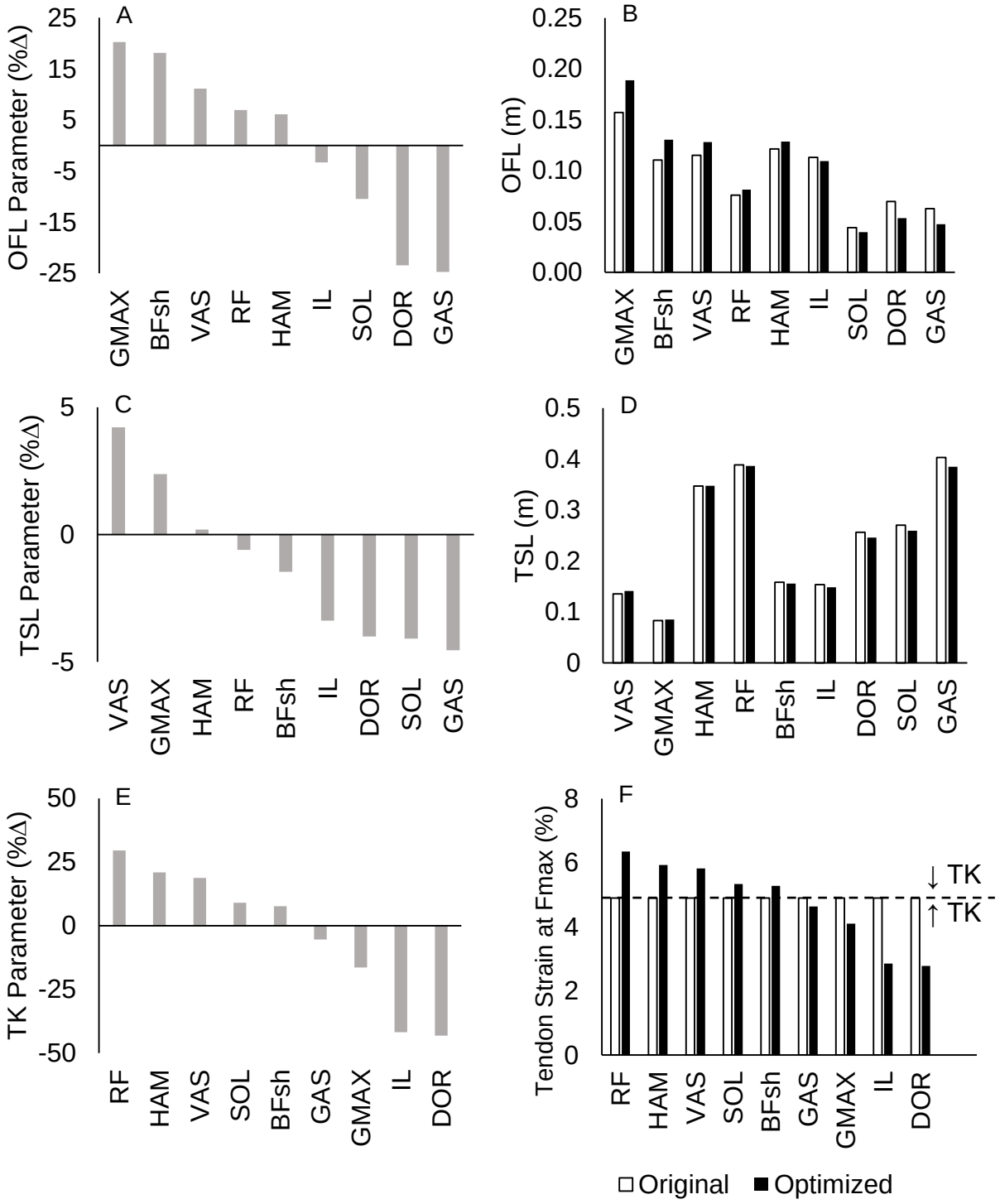

Figure 3.1 The relative and absolute changes in lower limb muscle-tendon unit properties when individually optimizing optimal muscle fiber length (OFL) (A & B), tendon slack length (TSL) (C & D), and tendon stiffness (TK) (E & F) during walking compared to the default model parameters. Tendon strain produced at maximum isometric force (F_{max}) below the dashed line represents a stiffer tendon (F). The vertical ranges for relative parameter outcomes match the size of the expanded parameter search space within the bilevel optimization. The represented muscle-tendon units include: hamstrings (HAM), biceps femoris short head (BFsh), gluteus maximus (GMAX),

iliopsoas (IL), rectus femoris (RF), vasti (VAS), gastrocnemius (GAS), soleus (SOL), dorsiflexors (DOR). Note the results for each parameter are presented in descending order.

Individually optimizing the MTU parameters resulted in lower whole-body neuromuscular effort during walking ranging from 16.6-41.0% lower than with the default parameter values(Table 3.2). Optimizing the MTU parameters also resulted in lower metabolic power during walking ranging from 0.2-9.5% lower compared to the default parameter values, even though the simulation objective function was defined to minimize neuromuscular effort, not metabolic cost (Table 3.2). Among the individually optimized parameters, neuromuscular effort was lowest when optimizing only OFL, and metabolic energy cost was lowest when only optimizing TSL. Simulations optimizing both OFL and TSL produced the greatest overall change in neuromuscular effort compared to the default parameter values but did not yield the greatest reduction in metabolic cost (Table 3.2).

Table 3.2 Change in neuromuscular effort and metabolic power when optimizing lower limb optimal muscle fiber length (OFL), tendon slack length (TSL), and tendon stiffness (TK) during walking compared to the default parameter values. The muscle-tendon interaction was further investigated by simultaneously optimizing OFL and TSL.

Optimized Parameter	Neuromuscular Effort (%Δ)	Metabolic Power (%Δ)
OFL	-41.0	-4.8
TSL	-37.6	-9.5
TK	-16.6	-0.2
OFL & TSL	-67.6	-5.5

While whole-body neuromuscular effort was lower when MTU parameters were individually optimized, the results across individual MTUs were different (Figure 3.2). Optimizing OFL produced lower neuromuscular effort in most MTUs compared to the default values (Figure 3.2 A & B). However, neuromuscular effort was lower in all MTUs when optimizing TSL

compared to the default parameter values (Figure 3.2 C & D). Optimizing TK resulted in the most variable changes among the MTUs, and the neuromuscular effort of nearly half the MTUs was greater than with the default parameter values (Figure 3.2 E & F).

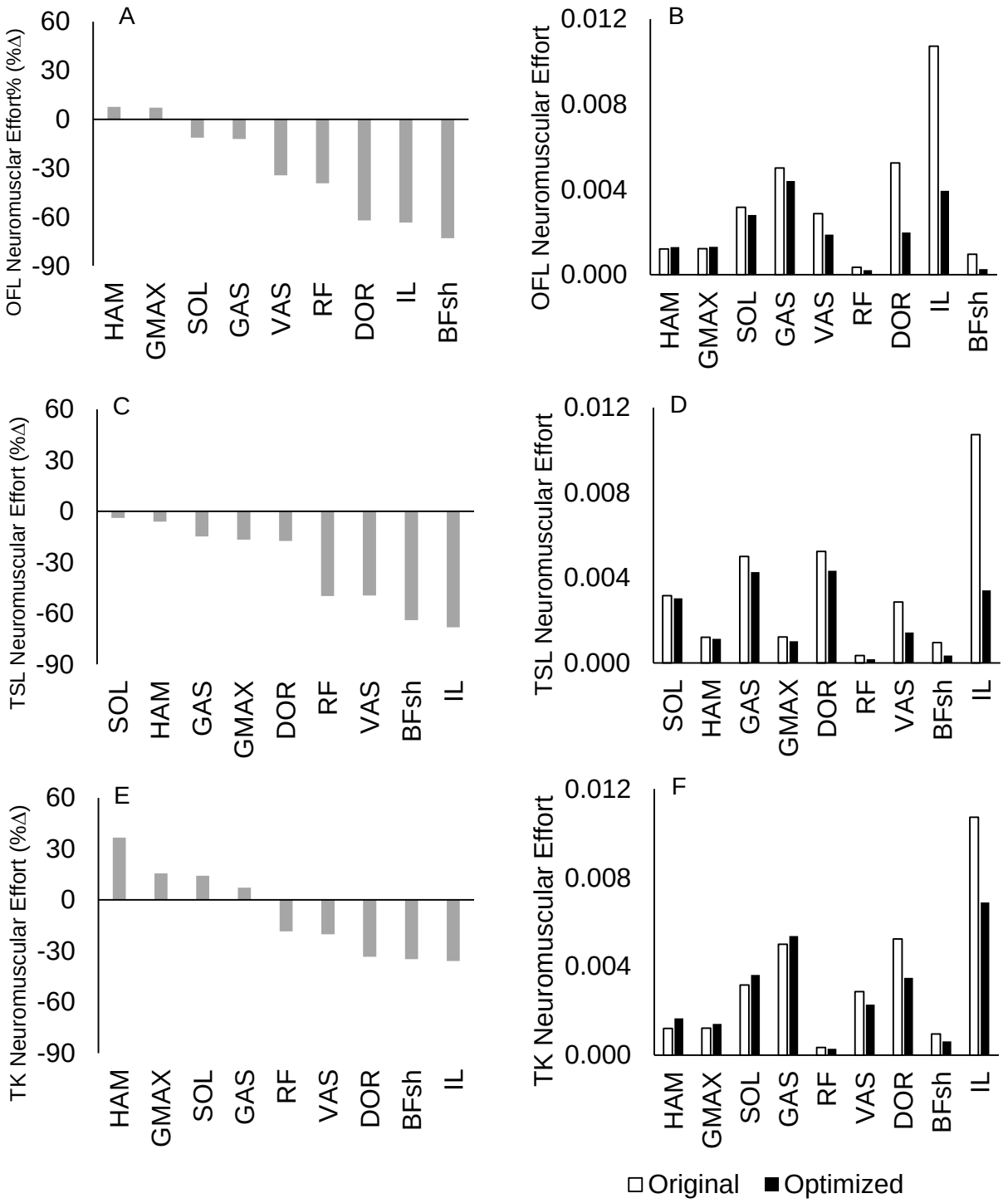

Figure 3.2 The relative and absolute changes in neuromuscular effort when individually optimizing optimal muscle fiber length (OFL) (A & B), tendon slack length (TSL) (C & D), and tendon stiffness (TK) (E & F) during walking compared to the default model parameters. Note the results for each parameter are presented in descending order. The represented muscle-tendon units include: hamstrings (HAM), biceps femoris short head (BFsh), gluteus maximus (GMAX),

iliopsoas (IL), rectus femoris (RF), vasti (VAS), gastrocnemius (GAS), soleus (SOL), dorsiflexors (DOR).

Individually optimizing the MTU parameters also lowered whole-body metabolic power, even though the simulation objective function was specifically defined to minimize neuromuscular effort. The metabolic energy cost of each MTU was not uniformly lower than the default model parameter values. (Figure 3.3). Across optimized parameters, the number of MTUs with greater metabolic power was comparable to the number of MTUs with lower metabolic power, respective to the default parameter values. However, greater metabolic power in some MTUs was more than offset by MTUs with lower metabolic power in order to achieve lower whole-body metabolic power. The biceps femoris short head consistently had the greatest relative percent decrease in metabolic power across all MTU parameters but minimally contributed to the absolute decrease in metabolic power (Figure 3.3).

,

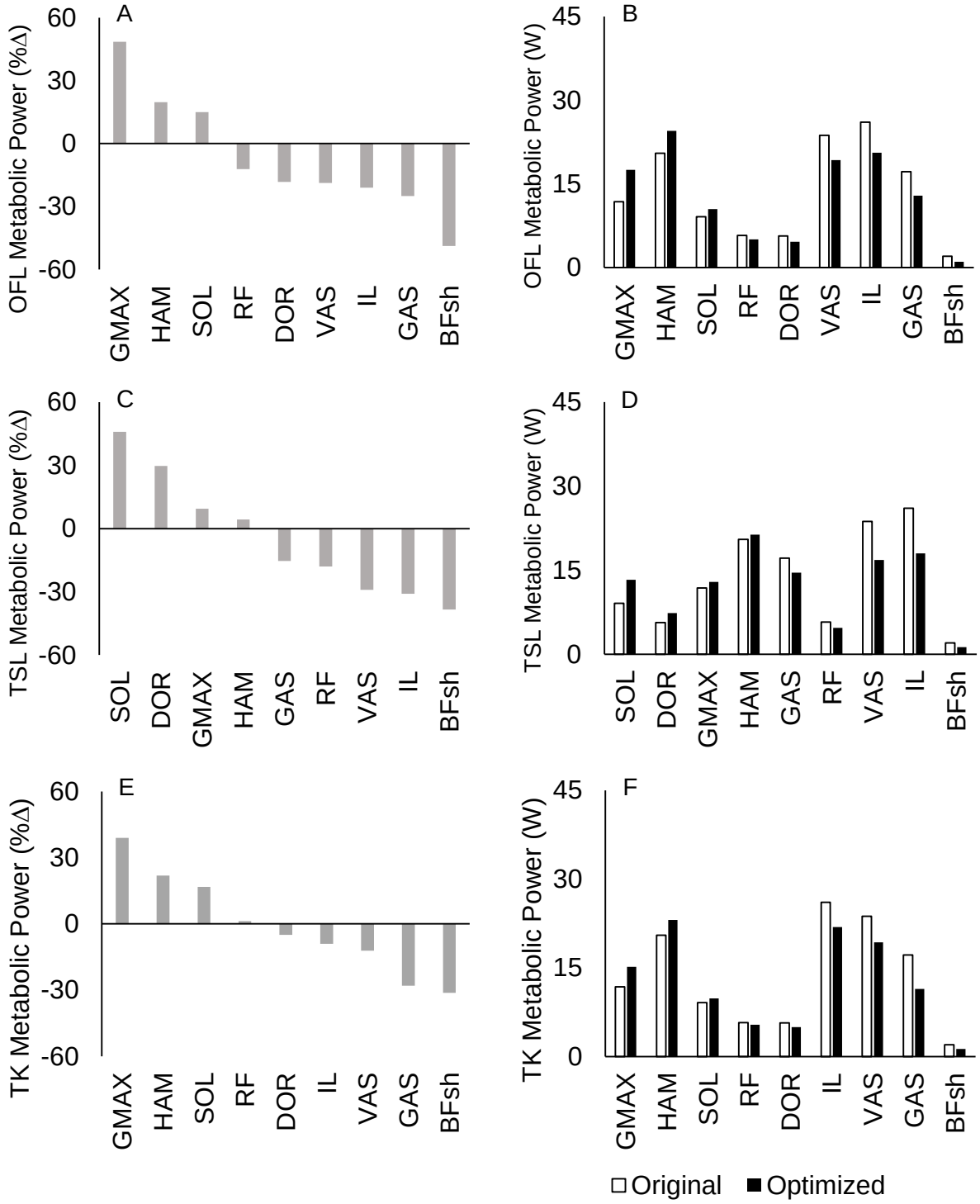

Figure 3.3 The relative and absolute changes in metabolic power when individually optimizing optimal muscle fiber length (OFL) (A & B), tendon slack length (TSL) (C & D), and tendon stiffness (TK) (E & F) during walking compared to the default model parameters. Note the results for each parameter are presented in descending order. The represented muscle-tendon units include: hamstrings (HAM), biceps femoris short head (BFsh), gluteus maximus (GMAX),

iliopsoas (IL), rectus femoris (RF), vasti (VAS), gastrocnemius (GAS), soleus (SOL), dorsiflexors (DOR).

Simultaneously optimizing OFL and TSL led to at least some degree of change in every MTU parameter compared to the default parameter values (Figure 3.4). The optimized MTU parameter values were each different, with some consistencies among muscle groups. OFL became longer in the HE and KE groups but shorter in the FX group (Figure 3.4 A & B). TSL became longer in the HE group but shorter in the KE and AE groups (Figure 3.4 C & D). The simultaneously optimized parameter values were generally similar to the individually optimized parameter values. However, the optimized OFL and TSL values for the biceps femoris short were transposed between optimizations.

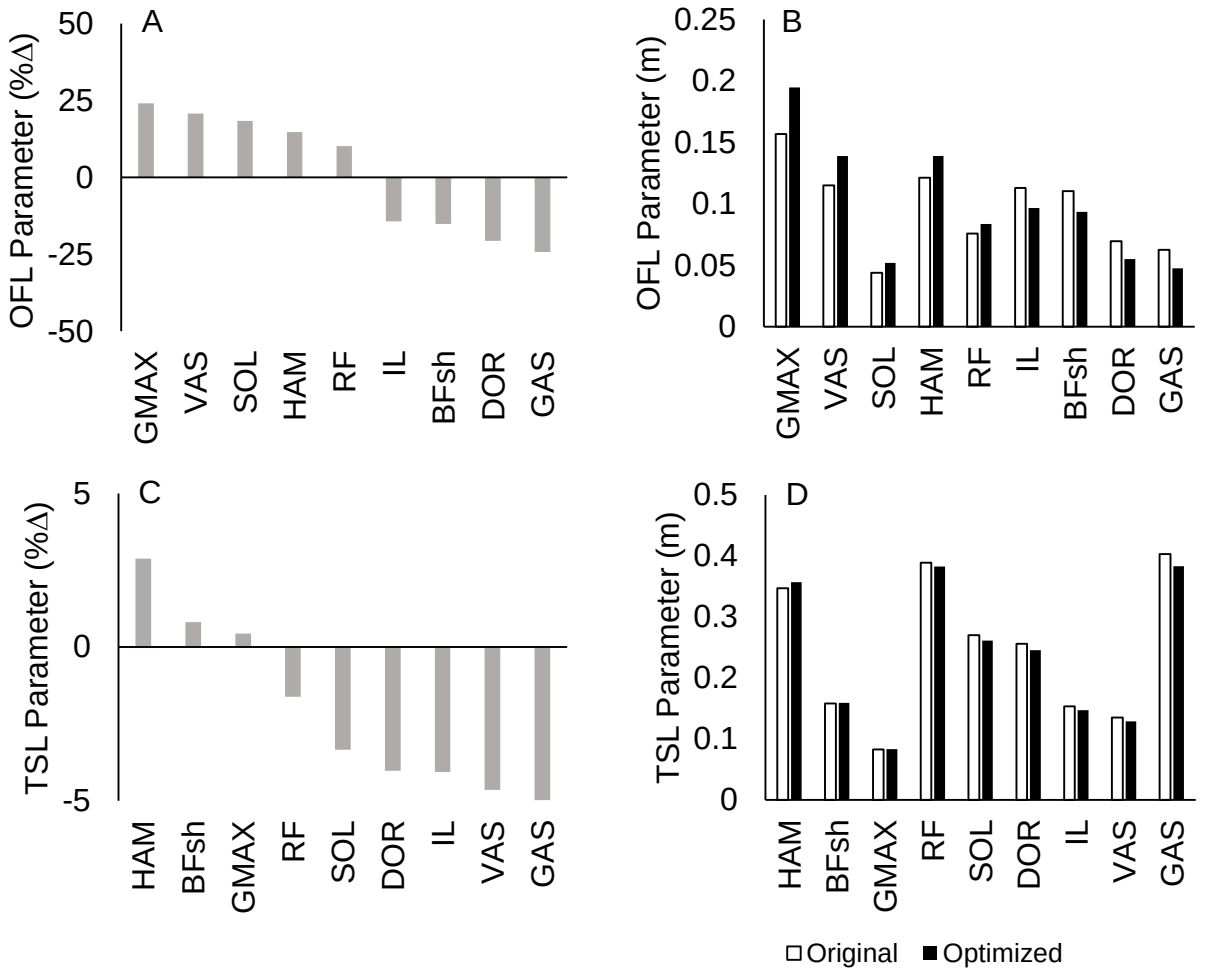

Figure 3.4 The relative and absolute changes in metabolic power when simultaneously optimizing optimal muscle fiber length (OFL) (A & B) and tendon slack length (TSL) (C & D) during walking compared to the default model parameters. Note the results for each parameter are presented in descending order. The represented muscle-tendon units include: hamstrings (HAM), biceps femoris short head (BFsh), gluteus maximus (GMAX), iliopsoas (IL), rectus femoris (RF), vasti (VAS), gastrocnemius (GAS), soleus (SOL), dorsiflexors (DOR).

Across individually optimized MTU parameters, lower whole-body neuromuscular effort and metabolic energy cost were primarily driven by lower demands in the FX group, at the relative and absolute levels (Figure 3.5). When OFL and TSL were simultaneously optimized, the relative and absolute neuromuscular effort in the FX and AE groups were the primary source of lower whole-body neuromuscular effort compared to the default parameter values (Figure 3.5 A & B).

However, the relative and absolute metabolic energy cost in the FX, AE, and KE groups were the primary source of lower whole-body metabolic energy cost compared to the default parameter values (Figure 3.5 C & D).

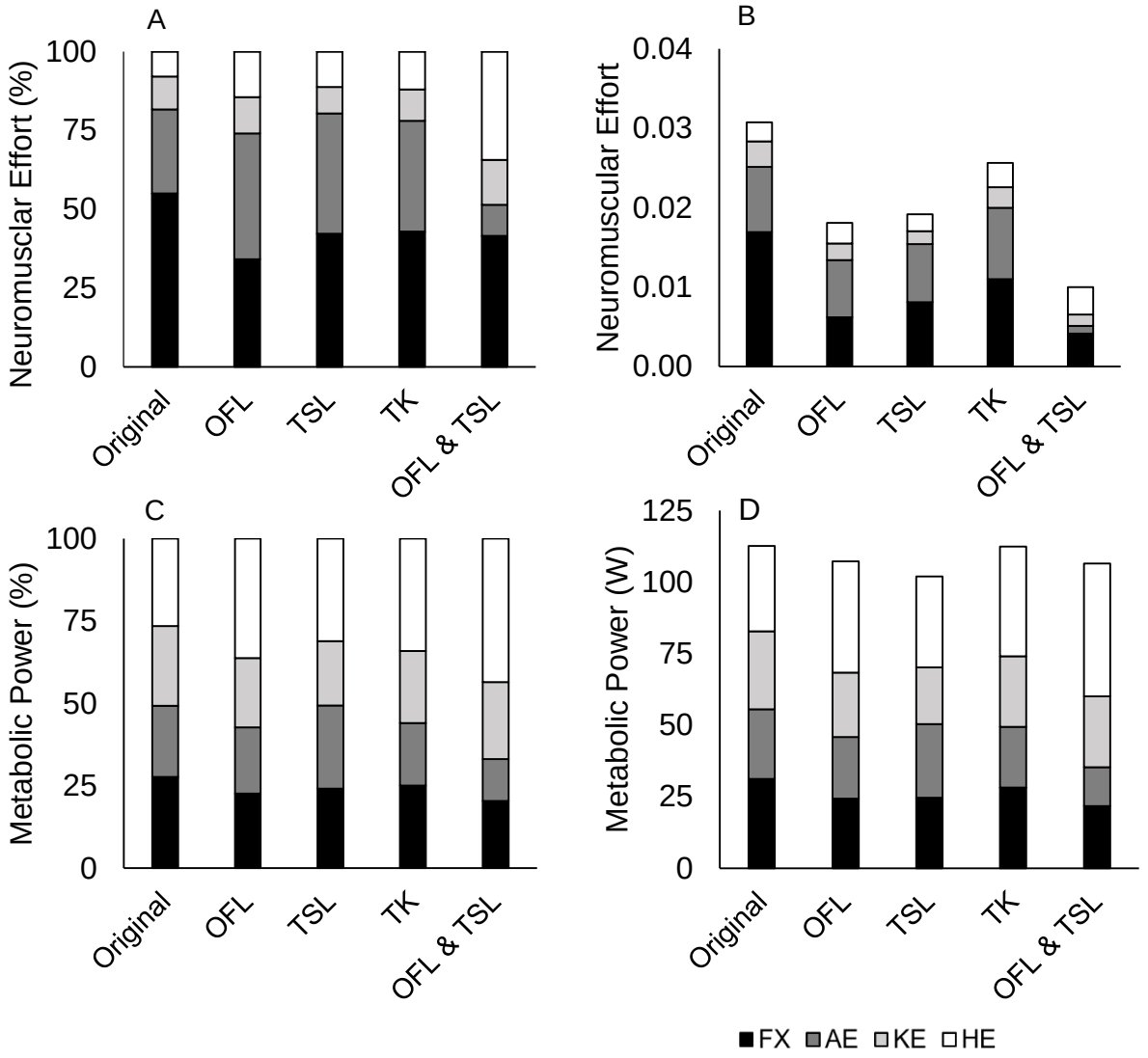

Figure 3.5 The relative and absolute neuromuscular effort (A & B) and metabolic power (C & D) for the optimized and default parameters for a single limb during a stride of walking across muscle groups. The flexors (FX) muscle group is the sum of the iliopsoas, biceps femoris short head, and dorsiflexors. The ankle extensors (AE) muscle group is the sum of the gastrocnemius and the soleus. The knee extensors (KE) muscle group is the sum of the rectus femoris and vasti. The hip extensors (HE) muscle group is the sum of the hamstring and gluteus maximus.

3.5 Discussion

The current study evaluated how OFL, TSL, and TK each affect the neuromuscular effort and metabolic energy cost of walking using musculoskeletal modeling and computer simulation. Properties of both muscle and tendon, as well as their interaction, play a critical role in determining the neuromuscular effort and metabolic energy cost of human locomotion. We hypothesized that individually optimizing these MTU parameters in a musculoskeletal model would permit walking with less neuromuscular effort and metabolic energy cost across muscles compared to the default parameter values. The findings of the current study partially support this hypothesis. Optimizing MTU parameters lowered whole-body neuromuscular effort and metabolic energy cost in comparison to the default parameter values. However, rather than a uniform reduction across all MTUs, the overall reductions in neuromuscular effort and metabolic energy cost were due to greater effort and cost in some MTUs that were more than offset by greater reductions in others. Among the muscle groups, reductions in the FX muscle group were the key component in reducing both whole-body neuromuscular effort and metabolic energy cost during walking.

All optimized MTU parameter values were at least somewhat different from the default musculoskeletal model parameter values. Some MTU parameters became longer or stiffer, whereas others became shorter or more compliant, but all values remained within anatomically realistic bounds [86], [112], [116] (Figure 3.1). The simulation objection function used in this study was defined to minimize neuromuscular effort, not metabolic energy cost, as minimizing effort generally produces more realistic simulations of human motion than minimizing metabolic cost [105], [175], [176]. In response, neuromuscular effort and metabolic energy cost were not uniformly lower across all individual MTUs despite lower whole-body values (Figure 3.2 & 3.3). There was no apparent connection between the change in length or stiffness for any of the

optimized MTU parameters and the resulting changes in neuromuscular effort or metabolic energy cost. For example, muscles with longer optimized OFLs were not linked to a specific uniform change in either neuromuscular effort or metabolic energy cost. However, the FX group was central to reducing both whole-body neuromuscular effort and metabolic energy cost during walking. Compared with the lower limb extensor muscles, the FX group minimally contributes to the support and propulsion of the body in walking and thus may have greater potential to reduce the demands during walking.

While neuromuscular effort and metabolic energy cost were both sensitive to individually optimized MTU parameters, neuromuscular effort was lowest when simultaneously optimizing OFL and TSL (Table 3.1). However, the reduction in metabolic energy cost when simultaneously optimizing OFL and TSL was similar to that obtained when optimizing only OFL, and not as low as when optimizing only TSL (Table 3.1). All MTU parameters impact the behavior of the MTU to varying degrees, yet prior research has consistently found that muscle force is most sensitive to TSL [106]–[109]. The results of the current study indicate TSL was also the parameter that had the greatest influence on the metabolic energy cost of walking. The muscle-tendon interaction is important for economic force production as mechanical work performed by the tendon offsets metabolically expensive muscle contractions and affects the operating length and velocity of the muscle fibers [12], [55].

Humans are recognized as economical walkers, possibly due to the evolutionary influence of bipedal walking [163], [164]. Preferred gait mechanics of human locomotion are often reported to correspond to observed minima in neuromuscular effort or metabolic energy cost [73]–[75]. Despite this propensity for minimum effort and cost, a previous study found that muscle activation patterns across lower limb MTUs were not all turned to be minimized at the preferred walking

speed [165]. In the current study, we similarly found lower limb MTU parameters were not specialized to minimize neuromuscular effort or metabolic energy cost in simulations at a typical walking speed. Both the findings in the literature and the current study add support to the notion that despite the presumed importance of bipedal walking in our evolution, human musculoskeletal structure and function are not specialized for level walking at the preferred speed. Instead, functional trade-offs may be present in order to accommodate different types of locomotion as well as other movements. For example, persistence hunting is purported to have played an important role in human postcranial musculoskeletal evolution and would have been selected for the ability to walk and run at a range of speeds in variable terrain over great distances [99]–[102].

During human locomotion, the central nervous system may prioritize minimizing neuromuscular effort and metabolic energy cost differently. Though these performance outcomes are related, it is important to note the differences between them. Computationally, neuromuscular effort is weighted equally among MTUs regardless of size, whereas, the metabolic energy contribution of each MTU is weighted by muscle volume [142], [144]. As a result, small muscles make the same contribution to the neuromuscular effort term as large muscles with the same excitation, but a few large muscles will generally dominate the metabolic energy cost simply due to volume. Additionally, the nonlinear relation of neuromuscular effort and the effectively linear relation of metabolic energy cost numerically contribute to the effectiveness of minimizing neuromuscular effort over metabolic energy cost. There is evidence to suggest humans may prioritize lower neuromuscular effort at the expense of greater metabolic energy expenditure [177]–[179]. In the current study, the change in whole-body and MTU-specific neuromuscular effort was not proportional or indicative of the subsequent change in metabolic energy cost. These

findings highlight the complex interaction and differences between the neuromuscular effort and metabolic energy cost during walking.

This study had several limitations. While OFL, TSL, and TK were individually optimized, only OFL and TSL were simultaneously optimized. Simultaneously optimizing all three parameters was computationally infeasible using our bilevel optimization approach. We focused on simultaneously optimizing OFL and TSL because each parameter individually had a large impact on neuromuscular effort and metabolic energy cost. Additionally, the current study only examined optimizing MTU parameters under a single condition, level ground walking at a typical speed. The optimized MTU parameter values found in the current study would likely not be the same for different locomotion speeds, inclines, or terrain.

In the current study, we used a novel approach to optimize the lower limb MTU parameters for human walking using bilevel optimization. The default musculoskeletal model MTU parameters were not optimal for minimizing whole-body neuromuscular effort, though the optimal parameter values all lay within anatomically realistic ranges. While humans are adept and economical at bipedal locomotion, our MTU anatomy is not exclusively tuned for walking at the preferred speed. Instead, our MTUs appear to be designed to accommodate a wide variety of movements.

3.6 Acknowledgments

We thank Varun Joshi for his contribution to data analysis.

Chapter 4 – Shear Wave Velocity of Lower Limb Tendons is not Correlated with Metabolic Power in Human Locomotion

4.1 Abstract

The mechanical behavior of spring-like tendons plays a crucial role in the mechanics and energetics of human locomotion by storing and releasing elastic strain energy and influencing muscle fiber behavior. Tendon stiffness is susceptible to long-term changes associated with aging and disease, and is responsive to physical training. It is challenging to directly measure tendon stiffness *in vivo*, but we can non-invasively estimate soft tissue stiffness using ultrasound shear wave elastography (SWE). While tendon stiffness is broadly relevant to a wide range of circumstances, our understanding of how lower limb tendon stiffness specifically affects whole-body and muscle performance is still incomplete. Therefore, this study aimed to explore the relationships between *in vivo* tendon stiffness of major lower limb tendons estimated using SWE and the metabolic energy cost of locomotion. This experimental approach was complemented by musculoskeletal simulations where tendon stiffness was systematically varied in a way that mirrored the experimental results. Thirty-six healthy young adults walked on a treadmill at slow, normal, and fast speeds, and ran at a slow speed while metabolic data were collected. Tendon stiffness was estimated in the tibialis anterior tendon, Achilles tendon, patellar tendon, and semitendinosus tendon at a resting slack length. Experimentally, net metabolic power for each locomotion speed was significantly different from every other speed (all $p<0.001$), and the mean shear wave velocity for each tendon was significantly different from every other tendon (all $p<0.001$). Lower limb tendon stiffness was not a significant predictor of the net metabolic power

at any of the examined locomotion speeds in the overall regression models (all $p>0.13$) or for any bivariate correlations (all $p>0.09$). The simulated results suggest MTU-specific correlations may be present but are not detectable at the whole-body level. Lower limb tendon stiffness was not related to the whole body metabolic cost of locomotion, which may partly reflect the limited sensitivity of individual muscle energy consumption to tendon stiffness for most muscle-tendon units.

4.2 Introduction

Tendons are a key element in the musculoskeletal system and are responsible for transferring the force generated by muscles to the skeleton. The properties of tendon, such as the stiffness, influence muscle contractile mechanics and ultimately determine the metabolic energy cost of movement. Tendon stiffness can impact the metabolic energy cost of muscle contraction in two ways: 1) through the operating length of the muscle fibers, affecting where on the force-length-velocity curve the muscle operates [48], and 2) storage and release of elastic strain energy, reducing the amount of metabolically expensive mechanical work done by the muscle fibers [45], [49], [54]. However, these different aspects of tendon function do not act in complete isolation from each other. The storage and release of elastic strain energy also affect muscle fiber dynamics because mechanical work done by the tendon affects the kinematics of the muscle fibers [45], [49], [54]. Thus, the tendon stiffness of the major lower limb muscle-tendon units (MTUs) will affect the muscle fiber dynamics and ultimately the metabolic energy cost of locomotion.

Tendon stiffness varies among individuals due to both external influences and internal physiological factors. For example, distance runners can exhibit increased Achilles tendon stiffness, which is correlated with greater running economy [38]. Whereas decreased tendon

stiffness, observed in older adults [32] and post-stroke patients [34], is accompanied by an elevated metabolic energy cost of walking [180], [181]. The detrimental changes in tendon properties that coincide with aging and disease can increase the difficulty and physical demands of everyday tasks like walking. More recently, tendon properties have become the target of genetic engineering approaches that have shown considerable improvements in physical performance [182], [183]. These approaches could potentially intervene in diseases affecting tendon properties and possibly restore the tendon. Changes in tendon stiffness ultimately affect the metabolic energy cost of movement through the muscle fiber dynamics. Thus, a fundamental understanding of how tendon stiffness affects MTU function and the associated metabolic energy cost is necessary for understanding how aging, exercise, and disease affect human locomotor performance across the lifespan.

Among mammals, bipedal walking and running are unique to humans and likely played an important role in our musculoskeletal evolution [163], [164]. As a result, human locomotion, specifically walking, is remarkably economical across the animal kingdom [184]. Among the many possible ways we could move, self-selected gait characteristics (speed, stride length, and stride frequency) generally minimize the metabolic energy cost of locomotion [84], [96], [185]. Despite this phenomenon, the neuromuscular activation of each leg muscle is not uniformly tuned to our preferred locomotion speeds, possibly due to an evolutionary adaptation to accommodate a wide range of locomotor behaviors [165].

While experimental studies often focus solely on the Achilles tendon (AT) due to its superficial nature and essential role in locomotion [61], [186], the ankle extensors represent only a small fraction of lower limb muscle mass [103] and account for only about 25% of the net metabolic energy cost of walking [143]. The effects of tendon stiffness across all major lower limb

MTUs on the metabolic energy cost of locomotion remains largely unknown. Investigating the tendon stiffness of additional major lower limb MTUs would provide further insights into the fundamental effects of the muscle-tendon interaction within the lower limb on the metabolic energetics of locomotion. Therefore, the present study took a broad and novel approach to examine how tendon stiffness throughout the lower limb impacts the metabolic energy cost of locomotion.

In order to directly measure tendon stiffness, tendon length must be measured when stretched by a force equal to the maximum isometric force (F_{max}) of the adjoining muscle to determine the force-displacement relation. Historically, tendon stiffness was estimated using cadaver specimens and animal models because the tendon could be dissected and manually lengthened, but this same process cannot be done in human participants [17], [187]. More recently, B-mode ultrasonography emerged as a commonplace and non-invasive method for estimating tendon stiffness by imaging the maximum displacement of the tendon during a ramped isometric contraction [23], [112]. However, this technique can be physically demanding for the participant and present a series of methodological obstacles to the experimenter. As an alternative, ultrasound shear wave elastography (SWE) requires minimal effort from the participant and is easier for the experimenter. SWE is a reliable and non-invasive approach to quantify the stiffness of tendon [127], [188]. SWE measurements can be used as experimental estimates of tendon stiffness, and can also be used in musculoskeletal modeling studies to further explore the impacts on MTU-specific metabolic energy cost.

Therefore, this study aimed to investigate the relationship between *in vivo* tendon stiffness of the major lower limb tendons, estimated using shear wave velocity (SWV), and the metabolic energy cost of locomotion. It was hypothesized that lower limb tendon stiffness will affect the metabolic energy cost of locomotion in an MTU-specific manner. For instance, we anticipated

greater AT stiffness would lead to a lower metabolic energy cost due to enhanced storage and release of elastic strain energy. However, we lack a theoretical basis or prior findings to predict the specific relationships for ankle dorsiflexors and knee flexors and extensors.

4.3 Methods

4.3.1 Participants

Thirty-six healthy young adults (18 male, 18 female; mean±SD: age: 25.7 ± 5.9 years, height: 1.7 ± 0.1 m, weight: 69.6 ± 14.7 kg) were recruited to participate in this study using flyers and an electronic database (UMHealthResearch). All participants reported no recent musculoskeletal injuries or diseases that would prevent walking or running, no history of lower limb tendon injuries, and no cardio-metabolic diseases. The International Physical Activity Questionnaire (IPAQ) short form [189] was used to assess the level of physical activity of participants and indicated participants were moderately active on average (2,850.5 ± 2,475.6 MET·min·wk-1). The protocol was approved by the Institutional Review Board (HUM00221589) at the University of Michigan. All participants provided written informed consent before participating.

4.3.2 Metabolic Data

Participants were instructed to fast and refrain from alcohol, caffeine, and smoking for at least three hours before the start of the session. We performed indirect calorimetry using a lightweight portable metabolic system (Cosmed K5, Rome, Italy) to measure the rate of consumed oxygen ($\dot{V}O_2$) and expired carbon dioxide ($\dot{V}CO_2$) gases. The resting metabolic energy cost was first measured during quiet sitting for five minutes and then quiet standing for five minutes.

Participants were acclimated to each of the tested walking and running speeds on the treadmill (FIT, Bertec Corporation, Columbus, OH, USA) while wearing the metabolic testing equipment for a total of five minutes. The metabolic energy cost was then measured while participants walked and ran on the treadmill at the four fixed speeds: slow walking - 1.0 m/s, normal walking - 1.3 m/s, fast walking - 1.6 m/s, and slow running - 2.5 m/s. Participants completed a five-minute trial at each speed and reached a steady state after three minutes [190]. Participants completed up to five minutes of seated rest between trials. The order of speeds was randomized.

The metabolic power of each trial was estimated from $\dot{V}O_2$ and $\dot{V}CO_2$ during the last two minutes of each trial [191]. The metabolic power during quiet standing was used to determine the net metabolic power of each locomotion trial.

4.3.3 Ultrasonography

Longitudinal ultrasound SWE images were obtained from tendons in four of the major lower limb MTUs: tibialis anterior tendon (TA), AT, patellar tendon (PT), and semitendinosus tendon (ST) (Supersonic Imagine Aixplorer system, Aix-en-Provence, France; SL18-5 transducer). SWE was performed after the completion of the metabolic data collection. The ultrasound region of interest was the middle third of the tendons, or the free tendon. The ultrasound transducer was aligned parallel to the tendon fascicles and visually identified using B-model ultrasonography. Participants were comfortably positioned on an athletic training table supine while imaging the anterior tendons and prone while imaging the posterior tendons. Only the dominant limb was assessed. We sought to reduce the passive tension in the tendons by standardizing the position of the joint corresponding to each targeted tendon (TA - 10° of dorsiflexion, AT - 20° of plantarflexion, PT - 0° of knee flexion, and ST - 120° of knee flexion).

The tendons were imaged in a randomized order. The same experimenter collected three images from each location across all participants.

SWV was analyzed in MATLAB (2022a, MathWorks, Natick, MA, USA) from SWE images using an established algorithm to ensure sufficient pixel quality [192], [193]. A single experimenter identified the region of the SWE images only containing the tendon of interest for analysis. The mean SWV of three images for each tendon was used for further analysis.

4.3.4 Statistical Analysis

The relationships among lower limb tendon stiffness, based on mean SWV, on the metabolic energy cost of locomotion at each speed were examined using multiple linear regression. One statistical model was used for each locomotion speed and the same four predictors were used in each model. Additionally, the relationship of each tendon on the metabolic energy cost of each speed was examined using bivariate correlations.

Differences in tendon mean SWV linked to sex and physical activity level (low, moderate, and high as determined by the IPAQ) were examined using independent t-tests using a Bonferroni correction.

4.3.5 Musculoskeletal Model

We used a two-dimensional musculoskeletal model [120] to simulate human locomotion with different tendon stiffness values. The model is summarized here and is described in more detail in Appendix A (Figure A.1). The sagittal plane model consisted of nine segments, 11 degrees of freedom, and 18 muscle-tendon unit actuators [155]. The foot-ground interaction was modeled using eight Hunt-Crossley contact elements under each foot [146].

We created thirty-six variations of the musculoskeletal model based on the variations in tendon stiffness in the thirty-six human participants in the current study. The musculoskeletal model characterizes tendon stiffness as strain produced at a force equal to the associated muscle F_{max}, which does not map directly to the experimental SWV estimates of tendon stiffness. Therefore, we adjusted the stiffness of the corresponding tendons in the model based on the percent difference from the mean SWV for each participant. Thus, the 36 musculoskeletal models were not meant to be subject-specific models capturing every detail of the individual subjects. Rather, the models reflected the ranges of muscle-specific variations in tendon stiffness in our sample, while holding all other model parameters constant.

4.3.6 Simulations

Predictive simulations of a step of walking and running at the same speeds observed experimentally were generated using OpenSim Moco 4.4 with a mesh interval density of size 50 [122] and MATLAB (2020a, MathWorks, Natick, MA, USA). The optimal control problem was set to minimize the sum of cubed muscle excitations, which has been shown to lead to realistic gait simulations [105]. Simulations were generated on a multicore computer workstation (Intel® CoreTM i9-7980XE CPU @ 2.6 GHz, 18-core processor, and 64 GB of RAM). Six cores were assigned to each optimal control problem, and three problems were solved in parallel. This parallel computing configuration was determined based on the outcomes of Chapter 2.

4.3.7 Evaluation

The simulated results were used to estimate the whole-body metabolic energy cost using a model of muscle energy consumption [144]. The MTU-specific metabolic energy was estimated

for the ankle flexors group (dorsiflexors), ankle extensors (gastrocnemius and soleus), knee flexors (biarticular hamstrings), and knee extensors (rectus femoris and vasti).

4.4 Results

Three participants were excluded from the analysis of slow running due to incomplete trials. The average net metabolic power increased as locomotion speed increased, and the net metabolic power for each locomotion speed was significantly different from every other speed (all $p<0.001$) (Figure 4.1A). The mean SWV for each tendon was significantly different from every other tendon (all $p<0.001$, Figure 4.1B). Moreover, the mean SWV of the ankle tendons (TA & AT) was significantly greater than for the knee tendons (PT & ST) ($p<0.001$). The mean SWV of the flexor tendons (TA & ST) was significantly greater than for the extensor tendons (AT & PT) ($p<0.001$). There were no significant differences between males and females (all $p>0.05$) or activity levels across all measurements (all $p>0.10$).

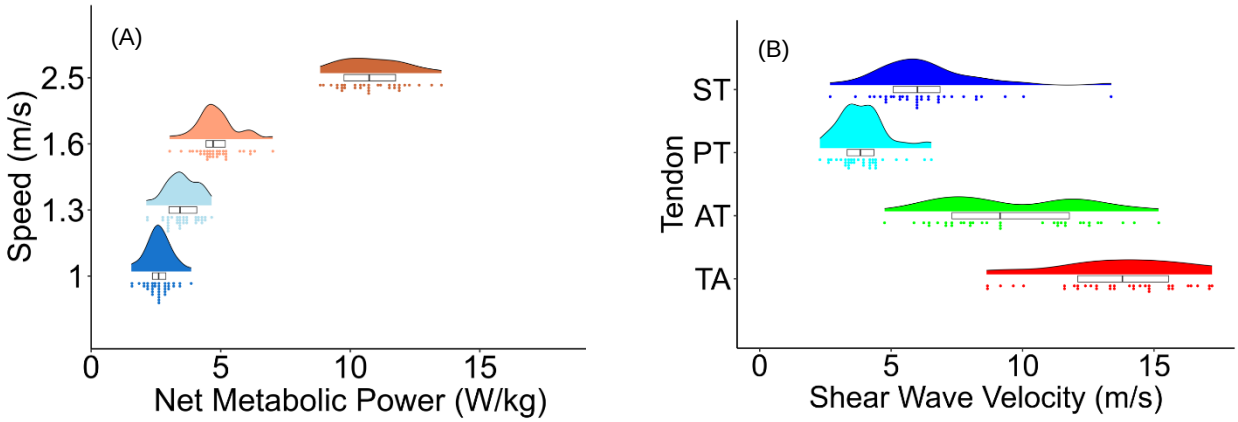

Figure 4.1 The net metabolic power during different speeds of locomotion (A) and mean shear wave velocity (SWV) of four major lower limb tendons (tibialis anterior tendon (TA), Achilles tendon (AT), patellar tendon (PT), and semitendinosus tendon (ST)) (B) in healthy young adults.

Mean SWV of the major lower limb knee and ankle tendons was not a significant predictor of the net metabolic power at any of the examined locomotion speeds in the overall multiple regression models (all $p>0.1$) (Table 4.1), or for any bivariate correlations (all $p>0.09$) (Figure 4.2 & Table 4.2).

Table 4.1 Multiple linear regression summary for each locomotor metabolic power outcome using the mean shear wave velocity of four major lower limb tendons (tibialis anterior tendon (TA), Achilles tendon (AT), patellar tendon (PT), and semitendinosus tendon (ST) as predictors.

Model	β	SE	*p*	Adjusted R^2
Slow (1.0 m/s)		0.50	0.44	<-0.01
Intercept	3.14	0.82		
TA	0.02	0.04	0.53	
AT	-0.04	0.03	0.20	
PT	-0.03	0.09	0.73	
ST	-0.05	0.05	0.25	
Normal (1.3 m/s)		0.64	0.89	-0.09
Intercept	3.43	1.06		
TA	0.03	0.05	0.52	
AT	-0.01	0.04	0.79	
PT	<-0.01	0.12	0.94	
ST	-0.03	0.06	0.58	
Fast (1.6 m/s)		0.84	0.84	-0.08
Intercept	6.04	1.38		
TA	-0.03	0.06	0.60	
AT	-0.06	0.05	0.29	
PT	0.02	0.15	0.89	
ST	-0.05	0.08	0.54	
Slow Run (2.5 m/s)		1.15	0.14	0.10
Intercept	10.43	1.89		
AT	0.18	0.09	0.06	
TA	-0.15	0.08	0.06	
PT	-0.24	0.23	0.30	
ST	0.05	0.11	0.62	

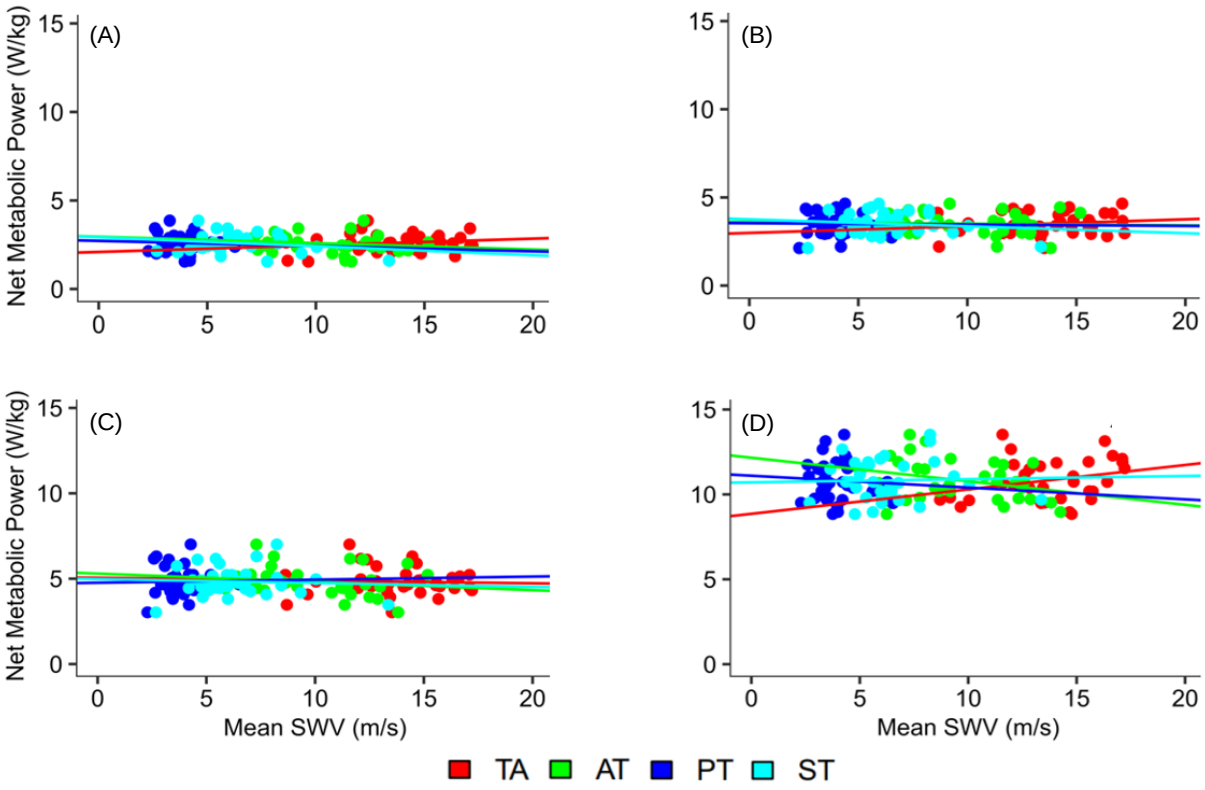

Figure 4.2 Bivariate correlations between the mean shear wave velocity (SWV) for the tibialis anterior tendon (TA), Achilles tendon (AT), patellar tendon (PT), and semitendinosus tendon (ST) and the net metabolic power during slow walking (A), normal walking (B), fast walking (C), and slow running (D).

Table 4.2 Bivariate correlations summary between the mean shear wave velocity for the tibialis anterior tendon (TA), Achilles tendon (AT), patellar tendon (PT), and semitendinosus tendon (ST) and the net metabolic power during slow walking, normal walking, fast walking, and slow running.

	β	SE	*p*	R^2	β	SE
Slow (1.0 m/s)						
	Predictor				Intercept	
TA	0.04	0.03	0.29	0.03	2.09	0.48
AT	-0.04	0.03	0.24	0.04	2.95	0.30
PT	-0.03	0.09	0.74	<0.01	2.72	0.36
ST	-0.05	0.04	0.24	0.04	2.92	0.28
Normal (1.3 m/s)						
	Predictor				Intercept	
TA	0.04	0.04	0.38	0.02	2.99	0.60
AT	-0.01	0.04	0.81	<0.01	3.60	0.38
PT	<-0.01	0.11	0.95	<0.01	3.54	0.44
ST	-0.04	0.05	0.46	0.02	3.76	0.35
Fast (1.6 m/s)						
	Predictor				Intercept	
TA	-0.02	0.06	0.78	<0.01	5.05	0.79
AT	-0.05	0.05	0.34	0.03	5.30	0.50
PT	0.02	0.15	0.90	<0.01	4.76	0.59
ST	-0.02	0.07	0.74	<0.01	4.98	0.46
Slow Run (2.5 m/s)						
	Predictor				Intercept	
TA	0.14	0.09	0.12	0.08	8.86	1.23
AT	-0.13	0.07	0.09	0.09	12.16	0.78
PT	-0.07	0.23	0.77	<0.01	11.10	0.93
ST	0.02	0.11	0.86	<0.01	10.71	0.70

Mean SWV was not uniform across the four major lower limb tendons within participants or at the joint level. The SWV in one tendon was not indicative of the SWV in any other tendon (Figure 4.3).

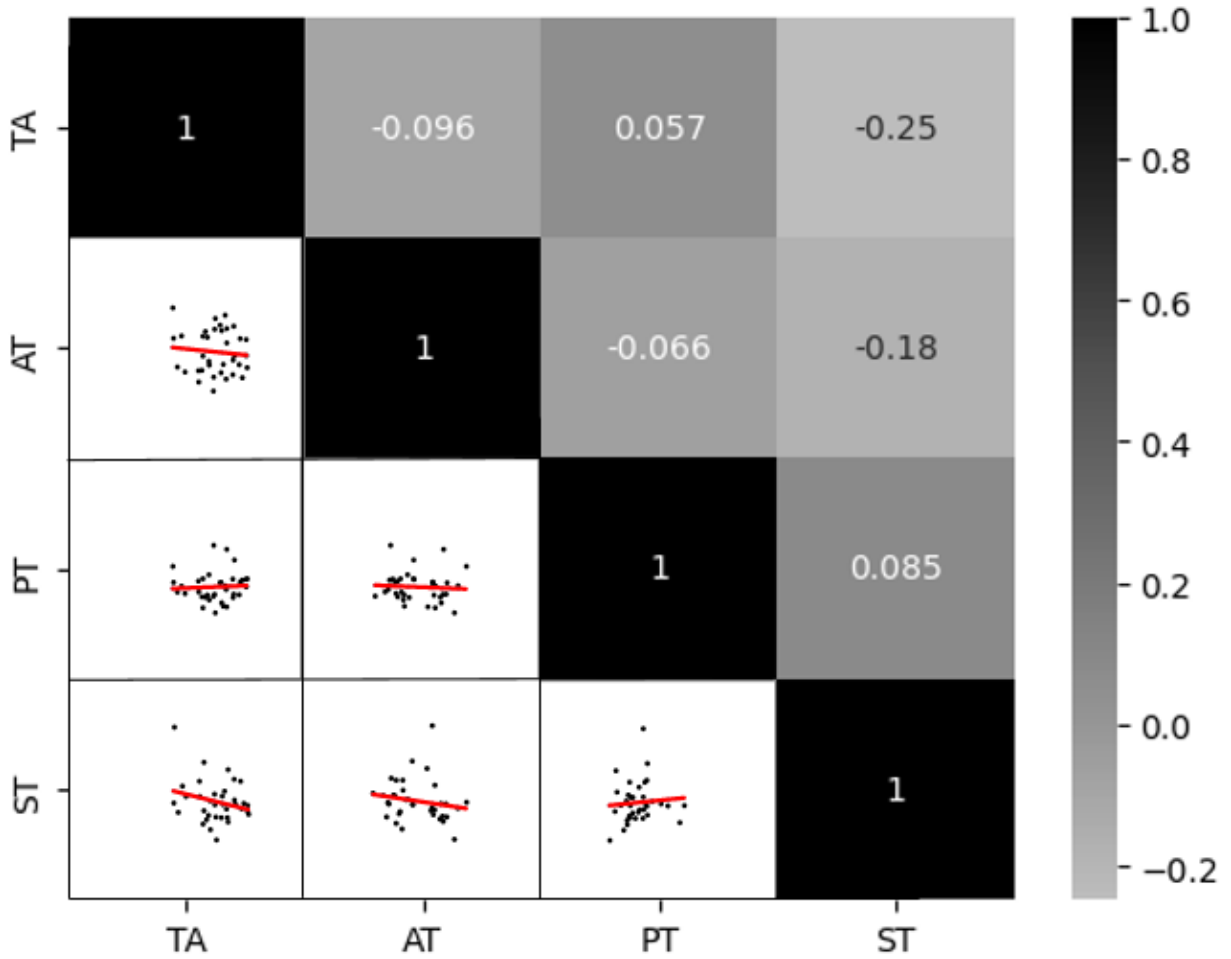

Figure 4.3 Correlation matrix for the mean shear wave velocity (SWV) of the major lower limbs tendons of four major lower limb tendons (tibialis anterior tendon (TA), Achilles tendon (AT), patellar tendon (PT), and semitendinosus tendon (ST)).

The gait simulations with different tendon stiffnesses followed the same general trends observed in the experimental data, with greater metabolic energy cost at faster speeds. The average predicted costs for the simulated gaits were slightly lower than the experimental means at each speed and there was less variation in metabolic cost at each speed in comparison to the experimental results (Figure 4.4). In most modeled MTU groups of interest, there was a weak correlation between tendon stiffness and the simulated muscle metabolic energy cost for each locomotion speed (Figure 4.5). The strongest relationship in the modeled MTUs was found in the ankle extensor muscles.

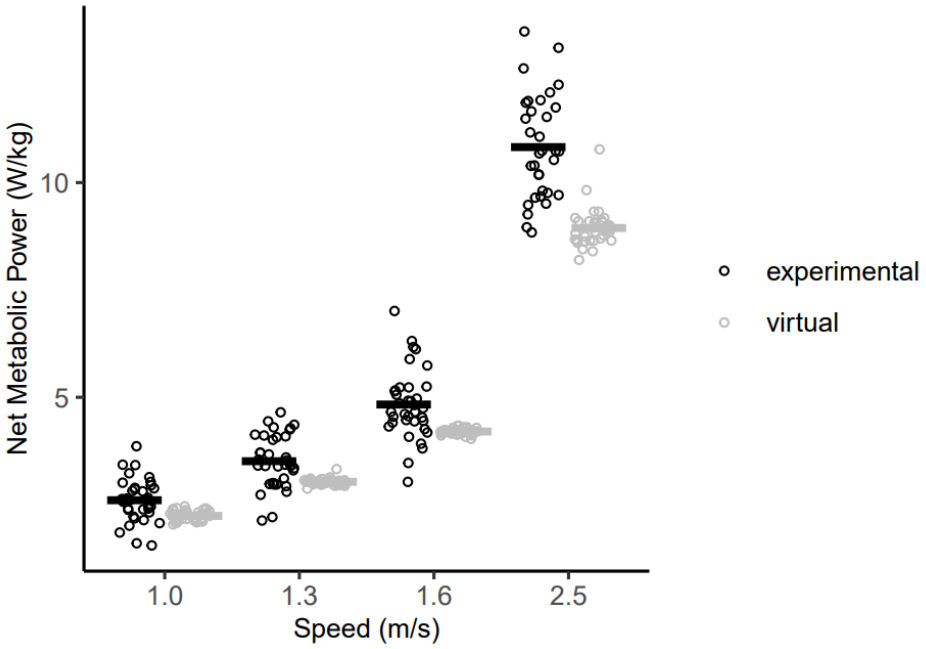

Figure 4.4 The distribution of net metabolic power for each locomotion speed for both the experimental and simulated experiments. Black circles are the whole-body net metabolic power of each human participant, and gray circles are the whole-body net metabolic power for each musculoskeletal model. The horizontal bars represent the mean for each sample.

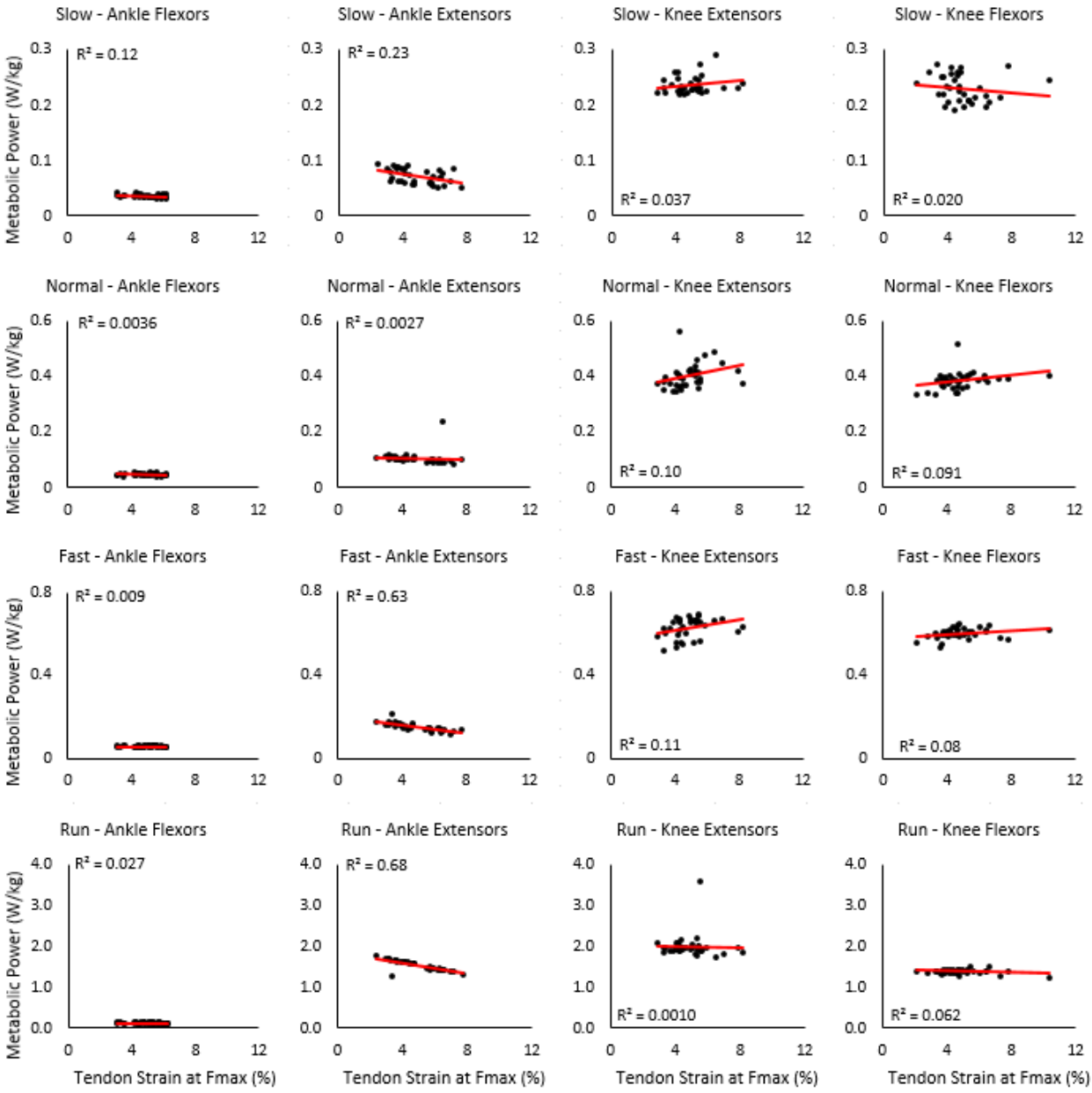

Figure 4.5 Bivariate correlations between tendon stiffness and the net metabolic power during slow walking, normal walking, fast walking, and slow running for the musculoskeletal modeling and simulation results. The musculoskeletal model represents tendon stiffness as strain produced at the maximum isometric force (F_{max}).

4.5 Discussion

We aimed to evaluate the relationship between *in vivo* tendon stiffness of the major lower limb tendons and the metabolic energy cost of locomotion using an integrated experimental and musculoskeletal simulation approach. We hypothesized that lower limb tendon stiffness would be related to the whole-body metabolic energy cost of locomotion in MTU-specific ways. For example, we expected greater AT stiffness would lead to a lower metabolic energy cost due to enhanced storage and release of elastic strain energy. However, we lacked a theoretical basis or prior findings to predict this relationship for the other tendons of the major MTUs. Our experimental findings do not support the specific hypothesis regarding AT stiffness, or a relationship with metabolic energy cost for any of the other tendons investigated here. Our simulation results indicate that the lack of relationships between tendon stiffnesses and whole-body metabolic energy cost may be due to there being only a weak association between tendon stiffness and individual MTU energy consumption, as well as a cancellation effect among certain MTUs (i.e., positive relation for one muscle offset by a negative relation for another muscle).

The current study used SWE to estimate the stiffness in four major lower limb tendons and then relate these measures to the metabolic energy cost of locomotion. We demonstrated lower limb tendon stiffness, estimated using SWE, is not associated with the metabolic energy cost at various speeds of walking or for slow running. There are several possibilities behind the lack of significant correlations between tendon stiffness and whole-body metabolic energy costs. We anticipated a relationship between tendon stiffness and the metabolic energy cost of location based on the findings of previous research [49], [53], [64]. However, it is plausible this relationship is simply non-existent. Tendon stiffness may not have a large effect on the metabolic energy cost of muscle contraction in locomotion. Moreover, we used SWE to estimate the stiffness of the tendon

at rest, but this static measurement may not translate to the mechanical behavior of the tendon during locomotion. It is possible that using a different technique to capture *in vivo* tendon stiffness may have identified a relationship between stiffness and metabolic energy cost during locomotion, though it remains possible this relationship still may not exist. Furthermore, correlations may be present at the MTU-specific level, though the impacts are not detectable at the whole-body level due to minimal overall contributions to whole-body metabolic energy cost. Alternatively, there may be opposing relationships among the MTUs, resulting in a negligible effect on whole-body metabolic energy cost.

The complementary musculoskeletal simulation approach allowed us to further investigate the metabolic energy cost of locomotion at the MTU-specific level with prescribed variations in tendon stiffness. The correlations between tendon stiffness and the MTU-specific metabolic energy cost were weak for most of the MTUs across the different gaits (Figure 4.5). In some cases, there were weak positive correlations between tendon stiffness and MTU-specific metabolic energy cost in some MTUs and weak negative correlations in others MTUs, which could result in cancellations at the whole-body level (Figure 4.5). AT stiffness had the strongest correlation with the MTU-specific metabolic energy cost, yet the change in the energy consumption by this one muscle group may be inconsequential at the whole-body level. Moreover, the observed positive correlation contradicts our expectation for the AT. Our assumption was that a spring-like tendon would store and release elastic strain energy, offsetting metabolically expensive mechanical demands of the plantar flexor muscle fibers [45], [49], [54], reducing the whole-body metabolic energy cost of locomotion. Our contrary results were, however, consistent with a recent simulation study that found that given a 25% stiffer Achilles tendon, the metabolic energy cost of the ankle extensors was 7% greater, but the whole-body metabolic energy cost was only 1.5% greater than

the default condition [117]. Thus, while AT stiffness was correlated with the metabolic energy consumed by the ankle extensors, the impact on whole-body metabolic energy cost is expected to be minimal. Both of these factors would limit any correlations between experimentally measured tendon stiffness and whole-body metabolic energy cost.

We found the mean SWV of the AT fell well within the expected range reported in the literature for healthy young adults [131], [194]–[197]. The mean SWV of the PT observed in the current study was slightly lower than most values reported in the literature but was generally within the expected range[135], [188], [197]–[200]. There are limited data on the mean SWV of the ST in the literature, though the values that are reported were greater than the results of the current study [201]. To our knowledge, no existing literature provides data for comparing *in vivo* SWV of the TA. Discrepancies between mean SWVs of the current and the literature are likely due to much of the literature measuring the tendons with some degree of passive strain. SWV is sensitive to passive tension [131], [196], and thus the tendons in the current study were imaged at joint angles intended to slacken the tendons which would result in lower SWV values.

Expanding our knowledge of the biomechanical function of tendons during human locomotion has broad applications in other fields of research, such as the design of human-integrated assistive robotic devices. Some powered prosthetic legs (e.g. [202]–[208]) and lower limb exoskeletons (e.g. [209]–[213]) are designed with series elastic actuators that share several similarities with the MTU [214]. However, the effectiveness of these series elastic actuators relies on appropriately tuning the stiffness of the elastic element with the demands of the task [205]–[208]. Though the use of series elastic actuators and proper tuning can reduce the mechanical demands of motorized systems, these systems are sensitive to locomotion variations other than preferred speed-level walking [205]–[208]. This concept complements the findings in the current

study; however, MTUs in humans are not readily modifiable for specific tasks. Moreover, these biologically inspired devices have the potential to reduce the burden and metabolic energy cost of human movement, which is important for amputees, individuals with movement disorders, and those who experience extreme physical demands.

There were several limitations to this study. SWE is limited in that it cannot capture the properties of the tissue during intermittent changes, such as those experienced by the MTUs during locomotion. Additionally, the maximum detectable SWV range is limited, making it challenging to examine fairly rigid tissues, such as tendons, except at rest with minimal passive tension. Although the leg was positioned to reduce passive tension while the tendons were imaged, some of the observed variations in tendon SWV may be due to inter-subject variability in tendon slack length. The current study examined only one running speed at a slow place; however, the advantage of storing and releasing elastic strain energy may be more pronounced at faster running speeds [186]. Moreover, there was no direct correspondence between tendon SWV and the representation of tendon stiffness within the musculoskeletal model. Therefore, the experimental measurements of tendon stiffness from the human participants were used to produce relative changes in tendon stiffness in the musculoskeletal model to investigate MTU-specific response.

The current study used experimental techniques in conjunction with musculoskeletal modeling and simulation to investigate the effects of lower limb tendon stiffness on the metabolic energy cost of walking and running. Despite including stiffness measures from several major knee and ankle flexor and extensor tendons, we did not observe any effect of lower limb tendon stiffness on the whole-body metabolic energy cost of walking or running. The simulation results indicate that the lack of significant relationships between the stiffness of individual tendons with whole-body metabolic cost may be due to weak correlations at the MTU level or trade-offs among MTUs.

It is difficult to link the characteristics of any element of the musculoskeletal system to whole-body metabolic cost in locomotion.

4.6 Acknowledgments

This work was funded by the University of Michigan Rackham Graduate Research Grant. We thank Lillian Bambacht, Wenxi Zhang, Varun Joshi, and Sheeba Davis for their assistance with data collection. We also thank David Lipps and Susann Wolfram for their assistance with the design of the study.

Chapter 5 – General Discussion and Conclusions

The primary objective of this dissertation was to explore the lower limb muscle-tendon unit (MTU) properties to gain a deeper understanding of the impacts on the mechanics and metabolic energy cost of human locomotion. The MTU functions as a biological motor and is essential for voluntary movement. However, the biomechanical properties of muscles and tendons can change over the lifespan, and thus impact the performance of the MTU. The impact of MTU properties on musculoskeletal function is poorly understood but has broad implications for understanding a range of phenomena including clinical gait disorders, human performance, and the evolution of human bipedalism. Herein, we present a broad and novel approach using a musculoskeletal modeling framework in isolation and integrated with traditional experimental techniques.

5.1 The role of parallel computing on musculoskeletal simulation computational performance

Optimal control musculoskeletal simulation is a valuable research approach capable of providing novel insights into several aspects of human movement. However, the high computational demand is a major limiting factor of this technique. Solving musculoskeletal simulation problems with OpenSim Moco [122] using parallel computing can potentially reduce the computational demand. Therefore, we thoroughly investigated how the number of processor cores in a single multicore computer interacts with musculoskeletal model complexity, movement task, initial guess type, and temporal mesh density to affect musculoskeletal simulation runtime and speed-up potential. The first study of this dissertation focused on achieving the computational

performance necessary to meet the demands of the remaining two studies, both in isolation and integrated with experimental data. We found parallel computing on a single multicore workstation can substantially improve the computational performance of solving optimal control simulations but was broadly problem specific. This investigation enabled us to perform studies that would have been computationally infeasible several decades ago. Multicore parallel computing reduces the computational demand of optimal control musculoskeletal simulations and enhances the feasibility as a research and clinical tool.

5.2 The role of optimal muscle-tendon unit properties in locomotor performance

The MTU is an important component of the musculoskeletal system responsible for generating and transmitting forces to produce movement. The structural features of the MTU are major determinants of the overall contractile behavior of muscle and the metabolic energy cost of movement but can change over the lifespan. We used optimal control musculoskeletal simulation to investigate the effects of optimal muscle fiber length, tendon slack length, and tendon stiffness on whole-body and muscle-specific locomotor performance. We found lower limb MTU parameters can be optimized to lower the whole-body neuromuscular and metabolic energy cost of human walking. However, reducing overall demands generally required greater neuromuscular effort or metabolic energy cost in some muscles that were offset by greater reductions in others. Although human walking is remarkably economical, the MTU parameters are not tuned to exclusively minimize the neuromuscular effort or metabolic cost of walking. MTU-specific performance outcomes may reflect evolutionary trade-offs associated with the need to perform tasks besides level walking. Continental migration and persistence hunting are widely acknowledged for their potential role in the development of bipedalism in human ancestors and the evolution of the postcranial musculoskeletal system. The ability to accommodate a range of

locomotor tasks, at the expense of being optimized for the task of level walking at a typical speed, may have been important for human survival and success as a species.

5.3 The role of *in vivo* lower limb tendon stiffness on the metabolic energy cost of locomotion

Spring-like tendons perform a key function in human locomotion by storing and releasing elastic strain energy, thus impacting muscle fiber behavior and metabolic energy cost. The effects of tendon stiffness across the major lower limb MTUs on the whole-body and MTU-specific metabolic energy cost of locomotion remains largely unknown but have broad implications for understanding a range of phenomena including clinical gait disorders, human performance, and the evolution of human bipedalism. We explored the relationships between *in vivo* tendon stiffness of major lower limb tendons using experimental techniques integrated with musculoskeletal simulation. Despite including measurements from several major knee and ankle flexor and extensor tendons, lower limb tendon stiffness was not associated with whole-body metabolic power during locomotion. Correlations may be present at the MTU-specific level but are not detectable at the whole-body level either due to minimal whole-body contributions or counteracting relationships among the MTUs. The simulations illustrate the lack of significant relationships between lower limb tendon stiffness and whole-body metabolic cost may be due to trade-offs at the MTU-specific level. Even so, it is difficult to link the characteristics of any element of the musculoskeletal system to whole-body metabolic cost in locomotion.

5.4 Challenging the role of spring-like tendons during locomotion

Chapter 3 optimized tendon stiffness in the lower limb MTUs during walking using musculoskeletal simulation and examined the subsequent anatomical and physiological changes. These parameters are easily modified in a musculoskeletal model, though not in human

participants. However, MTU properties can still be measured in human participants. Chapter 4 estimated tendon stiffness in human participants and used musculoskeletal simulation to better explain the experimental observations. Using this integrated approach added useful MTU-specific information to the study that could not be obtained experimentally. Chapters 3 and 4 examined lower limb tendon stiffness through different methods and both found tendon stiffness to have a negligible impact on the whole-body metabolic energy cost of locomotion. However, spring-like tendons are widely recognized as an important component of human locomotion that can potentially reduce the metabolic energy cost of locomotion. It may be possible the role of tendons and their spring-like behavior in locomotion across the lower limb have been overstated relative to the function of the ankle extensor MTUs during bounding gaits. The results provide a more comprehensive understanding of the inner workings of the MTU and also challenge our current understanding.

5.5 Future directions

Chapter 4 of this dissertation integrated experimental estimations of tendon stiffness with musculoskeletal simulation to isolate the impact of tendon stiffness on MTU-specific metabolic energy cost during locomotion. Other than tendon stiffness, the anatomical and physiological variations in the musculoskeletal system of the human participants were not present in the musculoskeletal models. Future studies could aim to create a more diverse subject-specific set of musculoskeletal models, rather than isolate a single MTU parameter. These additions may include but are not limited to experimental estimates of tendon slack lengths, muscle maximum isometric force, and maximum tendon displacement. In particular, estimating tendon stiffness through maximum displacement may better capture the dynamic properties of the tendon. Possibly pairing

this with dynamic ultrasound imaging during human locomotion may better explain how the muscle and tendon function and interact.

Appendix A

Here I describe in detail the two-dimension full-body musculoskeletal model used in Chapters 2, 3, and 4 by Nguyen et al., 2019 [120].

A1. Full-body Two-dimensional Musculoskeletal Model

The sagittal plane musculoskeletal model consisted of 9 rigid segments: pelvis, torso, right and left femur, tibia, talus, calcaneus, and toes. The torso-pelvis and subtalar joints were each rigidly fused. The 11 degrees of freedom included: pelvis translation and planar rotation and a single rotation at each hip, knee, ankle, and metatarsophalangeal joint. The 18 Hill-type muscle-tendon unit actuators (nine for each leg) [155]: the biarticular hamstrings (HAM), biceps femoris short head (BFsh), gluteus maximum (GMAX), iliopsoas (IL), rectus femoris (RF), vasti (VAS), gastrocnemius (GAS), soleus (SOL), and dorsiflexors (DOR). For simplicity, only the elastic component of the spring-like tendon is modeled in this muscle model.

The foot-ground interaction was modeled using eight Hunt Crossley contact elements under each foot [146].

A2. Muscle-tendon Unit Model Properties

The passive fiber forces used in the musculoskeletal model by Lai et al., 2017 [216] were incorporated to adjust tendon slack lengths as determined by static and dynamic data [217]. Optimal muscle fiber lengths and pennation angles were derived from cadaver data [103]. Muscle

volumes and physiological cross-sectional areas (PSCA) were derived from the MRI data of young, healthy subjects [218].

A3. Tendon Stiffness

The level of tendon stiffness cannot be readily altered in human subjects but can be within a musculoskeletal model. Tendon strain was defined in the model as the relative elongation produced at maximum isometric force (F_{max}) and was consistently varied between 0 and 20% across all muscles in the model. This is typically set to 4.9% at F_{max} based on *in vivo* measurements of Achilles tendon strain using ultrasonography [23], [116]. This characteristic was altered directly in the musculoskeletal model as a property of the tendon force-length curve within the muscle model.

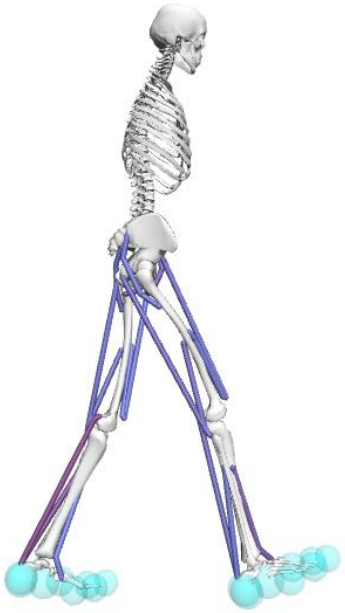

Figure A.1 The two-dimensional musculoskeletal model stance phase of walking. This model was used in Chapters 2, 3, and 4.

References

[1] A. V. Hill, “The heat of shortening and the dynamic constants of muscle,” *Proceedings of the Royal Society B: Biological Sciences*, vol. 126, no. 843, pp. 136-195, 1938.

[2] A. F. Huxley and R. M. Simmons, “Proposed mechanism of force generation in striated muscle,” *Nature*, vol. 233, pp. 533-538, 1971.

[3] K. A. Edman, G. Elzinga, and M. I. Noble, “Enhancement of mechanical performance by stretch during tetanic contractions of vertebrate skeletal muscle fibres,” *The Journal of Physiology*, vol. 281, no. 1, pp. 139-155, 1978.

[4] W. O. Fenn and B. S. Marsh, “Muscular force at different speeds of shortening,” *The Journal of Physiology*, vol. 85, no. 3, pp. 277-297, 1935.

[5] R. I. Griffiths, “Shortening of muscle fibres during stretch of the active cat medial gastrocnemius muscle: the role of tendon compliance,” *The Journal of Physiology*, vol. 436, no. 1, pp. 219-236, 1991.

[6] A. V. Hill, “The mechanics of voluntary muscle,” *The Lancet*, vol. 258, no. 6691, pp. 947-951, 1951.

[7] B. Katz, “The relation between force and speed in muscular contraction,” *The Journal of Physiology*, vol. 96, no. 1, pp. 45-64, 1939.

[8] D. E. Rassier, B. R. MacIntosh, and W. Herzog, “Length dependence of active force production in skeletal muscle,” *Journal of Applied Physiology*, vol. 86, no. 5, pp. 1445-1457, 1999.

[9] G. C. Joyce, P. M. H. Rack, and D. R. Westbury, “The mechanical properties of cat soleus muscle during controlled lengthening and shortening movements,” *The Journal of Physiology*, vol. 204, no. 2, pp. 461-474, 1969.

[10] Y. Kawakami, Y. Ichinose, and T. Fukunaga, “Architectural and functional features of human triceps surae muscles during contraction,” *Journal of Applied Physiology*, vol. 85, no. 2, pp. 398-404, 1998.

[11] J. M. Winters and S. L-Y. Woo. *Multiple Muscle Systems*. Springer New York, NY, 1990.

[12] B. C Abbott, B. Bigland, and J. M. Ritchie, “The physiological cost of negative work,” *The Journal of Physiology*, vol. 117, no. 3, pp. 380-390, 1952.

[13] A. M. Gordon, A. F. Huxley, and F. J. Julian, “Tension development in highly stretched vertebrate muscle fibres,” *The Journal of Physiology*, vol. 184, no. 1, pp. 143-169, 1966.

[14] T. W. Ryschon, M. D. Fowler, R. E. Wysong, A. -R. Anthony, and R. S. Balaban, “Efficiency of human skeletal muscle in vivo: comparison of isometric, concentric, and eccentric muscle action,” *Journal of Applied Physiology*, vol. 83, no. 3, pp. 867-874, 1997.

[15] A. V. Hill, “The mechanics of active muscle,” *Proceedings of the Royal Society B: Biological Sciences*, vol. 141, no. 902, pp. 104-117, 1952.

[16] F. J. Julian and D. L. Morgan, “Intersarcomere dynamics during fixed-end tetanic contractions of frog muscle fibres,” *The Journal of Physiology*, vol. 293, no. 1, pp. 365-378, 1979.

[17] R. F. Ker, R. McN. Alexander, and M. B. Bennett, “Why are mammalian tendons so thick?,” *Journal of Zoology*, vol. 216, no. 2, pp. 309-324, 1988.

[18] J. Diamant, A. Keller, E. Baer, M. Litt, and R. G. C. Arridge, “Collagen; ultrastructure and its relation to mechanical properties as a function of ageing,” *Proceedings of the Royal Society B: Biological Sciences*, vol. 180, no. 1060, pp. 293-315, 1972.

[19] B. J. Rigby, N. Hirai, J. D. Spikes, and H. Eyring, “The mechanical properties of rat tail tendon,” *Journal of General Physiology*, vol. 43, no. 2, pp. 265-283, 1959.

[20] A. Viidik, “Simultaneous mechanical and light microscopic studies of collagen fibers,” *Zeitschrift für Anatomie und Entwicklungsgeschichte*, vol. 136, pp. 204-212, 1972.

[21] M. B. Bennett, R. F. Ker, N. J. Dimery, and R. McN. Alexander, “Mechanical properties of various mammalian tendons,” *Journal of Zoology*¸ vol. 209, no. 4, pp. 537-548, 1986.

[22] K. Kubo, Y. Kawakami, and T. Fukunaga, “Influence of elastic properties of tendon structures on jump performance in humans,” *Journal of Applied Physiology*, vol. 87, no. 6, pp. 2090-2096, 1999.

[23] C. N. Maganaris and J. P. Paul, “Tensile properties of the in vivo human gastrocnemius t A. Viidik, L. Sandqvist, and M. Mägi, “Influence of postmortal storage on tensile strength characteristics and histology of rabbit ligaments,” *Acta Orthopaedica Scandinavica*, vol. 36, no. 79, pp. 3-38, 1965.

[25] S. L. Y. Woo, M. A. Ritter, D. Amiel, T. M. Sanders, M. A. Gomez, S. C. Kuei, S. R. Garfin, and W. H Akeson, “The biomechanical and biochemical properties of swine tendons — Long term effects of exercise on the digital extensors,” *Connective Tissue Research*, vol. 7, no. 3, pp. 177-183, 1980.

[26] N. D. Reeves, “Adaptation of the tendon to mechanical usage,” *Journal of Musculoskeletal and Neuronal Interactions*, vol. 6, no. 2, pp. 174-180, 2006.

[27] R. McN. Alexander, “Tendon elasticity and muscle function,” *Comparative Biochemistry and Physiology Part A: Molecular & Integrative Physiology*, vol. 133, no. 4, pp. 1001-1011, 2002.

[28] U. Proske and D. L. Morgan, “Tendon stiffness: Methods of measurement and significance for the control of movement. A review,” *Journal of Biomechanics,* vol. 20, no. 1, pp. 75-82, 1987.

[29] T. J. Roberts and R. L. Marsh, “Probing the limits to muscle-powered accelerations: Lessons from jumping bullfrogs,” *Journal of Experimental Biology,* vol. 206, no. 15, pp. 2567-2580, 2003.

[30] P. Blanpied and G. L. Smidt, “The difference in stiffness of the active plantarflexors between young and elderly human females,” *Journal of Gerontology,* vol. 48, no. 2, pp. M58-M63, 1993.

[31] K. Kubo, H. Kanehisa, M. Miyatani, M. Tachi, and T. Fukunaga, “Effect of low-load resistance training on the tendon properties in middle-aged and elderly women,” *Acta Physiologica Scandinavica,* vol. 178, no. 1, pp. 25-32, 2003.

[32] G. L. Onambele, M. V. Narici, and C. N. Maganaris, “Calf muscle-tendon properties and postural balance in old age,” *Journal of Applied Physiology,* vol. 100, no. 6, pp. 2048-2056, 2006.

[33] C. N. Maganaris, N. D. Reeves, J. Rittweger, A. J. Sargeant, D. A. Jones, K. Gerrits, and A. De Haan, “Adaptive response of human tendon to paralysis,” *Muscle and Nerve*, vol. 33, no. 1, pp. 85-92, 2006.

[34] H. Zhao, Y. Ren, Y.-N. Wu, S. Q. Liu, and L.-Q. Zhang, “Ultrasonic evaluations of Achilles tendon mechanical properties poststroke,” *Journal of Applied Physiology*, vol. 106, no. 3, pp. 843-849, 2009.

[35] S. Arya and K. Kulig, “Tendinopathy alters mechanical and material properties of the Achilles tendon,” *Journal of Applied Physiology,* vol. 108, no. 3, pp. 670-675, 2010.

[36] K. Kubo, H. Akima, M. Kouzaki, M. Ito, Y. Kawakami, H. Kanehisa, and T. Fukunaga, “Changes in the elastic properties of tendon structures following 20 days bed-rest in humans,” *European Journal of Applied Physiology,* vol. 83, pp. 463-468, 2000.

[37] C. I. Buchanan and R. L. Marsh, “Effects of long-term exercise on the biomechanical properties of the Achilles tendon of guinea fowl,” *Journal of Applied Physiology,* vol. 90, no. 1, pp. 164-171, 2001.

[38] J. R. Fletcher, S. P. Esau, and B. R. MacIntosh, “Changes in tendon stiffness and running economy in highly trained distance runners,” *European Journal of Applied Physiology,* vol. 110, no. 5, pp. 1037-1046, 2010.

[39] K. Kubo, H. Kanehisa, M. Ito, T. Fukunaga, and K. Kubo, “Effects of isometric training on the elasticity of human tendon structures in vivo,” *Journal of Applied Physiology*, vol. 91, no. 1, pp. 26-32, 2001.

[40] N. D. Reeves, C. N. Maganaris, and M. V. Narici, “Effect of strength training on human patella tendon mechanical properties of older individuals,” *Journal of Physiology*, vol. 548, no. 3. pp. 971-981, 2003.

[41] T. Fukunaga, K. Kubo, Y. Kawakami, S. Fukashiro, H. Kanehisa, and C. N. Maganaris, “In vivo behaviour of human muscle tendon during walking,” *Proceedings of the Royal Society B: Biological Sciences*, vol. 268, no. 1464, pp. 229-233, 2001.

[42] K. Kubo, H. Kanehisa, D. Takeshita, Y. Kawakami, S. Fukashiro, and T. Fukunaga, “*In vivo* dynamics of human medial gastrocnemius muscle-tendon complex during stretch-shortening cycle exercise,” *Acta Physiologica Scandinavica*, vol. 170, no. 2, pp. 127-135, 2008.

[43] B. I. Priiutsky, W. Herzog, T. R. Leonard, and T. L. Allinger, “Role of the muscle belly and tendon of soleus, gastrocnemius, and plantaris in mechanical energy absorption and generation during cat locomotion,” *Journal of Biomechanics*, vol. 29, no. 4, 417-434, 1996.

[44] J. A. Hoffer, A. A. Caputi, I. E. Pose, and R. I. Griffiths, “Roles of muscle activity and load on the relationship between muscle spindle length and whole muscle length in the freely walking cat,” *Progress in Brain Research*, vol. 80, pp. 75-85, 1989.

[45] T. J. Roberts, “The integrated function of muscles and tendons during locomotion,” *Comparative Biochemistry and Physiology Part A: Molecular & Integrative Physiology*, vol. 133, no. 4, pp. 1087-1099, 2002.

[46] G. A. Lichtwark and A. M. Wilson, “*In vivo* mechanical properties of the human Achilles tendon during one-legged hopping,” *Journal of Experimental Biology*, vol. 208, no. 24, pp. 4715-4725, 2005.

[47] H. S. Gasser and A. V. Hill, “The dynamics of muscular contraction,” *Proceedings of the Royal Society B: Biological Sciences*, vol. 96, no. 678, pp. 398-437, 1924.

[48] E. Caldwell, “Tendon elasticity and relative length: Effects on the Hill two-component Muscle Model,” *Journal of Applied Biomechanics*, vol. 11, no. 1, pp. 1-24, 1995.

[49] G. A. Cavagna and M. Kaneko, “Mechanical work and efficiency in level walking and running,” *The Journal of Physiology*, vol. 268, no. 2, pp. 467-481, 1977.

[50] A. L. Hof, B. A. Geelen, and J. W. van den Berg, “Calf muscle moment, work and efficiency in level walking; Role of series elasticity,” *Journal of Biomechanics*, vol. 16, no. 7, pp. 523-537, 1983.

[51] M. Ishikawa, P. V. Komi, M. J. Grey, V. Lepola, and G.-P. Bruggemann, "Muscle-tendon interaction and elastic energy usage in human walking," *Journal of Applied Physiology*, vol. 99, no. 22, pp. 603-608, 2005.

[52] M. Ishikawa, J. Pakaslahti, and P. V. Komi, "Medial gastrocnemius muscle behavior during human running and walking," *Gait and Posture*, vol. 25, no. 3, pp. 380-384, 2007.

[53] R. McN. Alexander and H. C. Bennet-Clark, "Storage of elastic strain energy in muscle and other tissues," *Nature*, vol. 265, pp. 114-117, 1977.

[54] N. C. Holt, T. J. Roberts, and G. N. Askew, "The energetic benefits of tendon springs in running: Is the reduction of muscle work important?," *Journal of Experimental Biology*, vol. 217, no. 24, pp. 4365-4371, 2014.

[55] R. Margaria, "Positive and negative work performances and their efficiencies in human locomotion," *European Journal of Applied Physiology*, vol. 25, pp. 339-351, 1968.

[56] R. McN. Alexander and R. F. Ker, "The architecture of leg muscles," *Multiple Muscle* Systems, pp. 568-577, 1990.

[57] A. A. Biewener, "Muscle function *in vivo*: A comparison of muscles used for elastic energy savings versus muscles used to generate mechanical power," *Integrative & Comparative Biology*, vol. 38, no. 4, pp.703-717, 1998.

[58] A. A. Biewener, "Muscle and tendon contributions to force, work, and elastic energy savings: A comparative perspective," *Exercise and Sport Sciences Reviews*, vol. 28, no. 3, pp. 99-107, 2000.

[59] J. A. Friederich and R. A. Brand, "Muscle fiber architecture in the human lower limb," *Journal of Biomechanics*, vol. 23, no. 1, pp. 91-95, 1990.

[60] F. C. Anderson and M. G. Pandy, "Storage and utilization of elastic strain energy during jumping," *Journal of Biomechanics*, vol. 26, no. 12, pp. 1413-1427, 1993.

[61] G. A. Lichtwark and A. M. Wilson, "Optimal muscle fascicle length and tendon stiffness for maximising gastrocnemius efficiency during human walking and running," *Journal of Theoretical Biology*, vol. 252, no. 4, pp. 662-673, 2008.

[62] T. Fukunaga, Y. Kawakami, K. Kubo, and H. Kanehisa, "Muscle and tendon interaction during human movements," *Exercise and Sport Sciences Reviews*, vol. 30, no. 3, pp. 106-110, 2002.

[63] G. A. Lichtwark, K. Bougoulias, and A. M. Wilson, "Muscle fascicle and series elastic element length changes along the length of the human gastrocnemius during walking and running," *Journal of Biomechanics*, vol. 40, no. 1, pp. 157-164, 2007.

[64] R. McN. Alexander, "Energy-saving mechanisms in walking and running," *Journal of Experimental Biology*, vol. 160, no. 1, 55-69, 1991.

[65] R. McN. Alexander, "Elastic energy stores in running vertebrates," *Integrative & Comparative Biology*, vol. 24, no. 1, pp. 85-94, 1984.

[66] G. A. Cavagna, N. C. Heglund, and C. R. Taylor, "Mechanical work in terrestrial locomotion: Two basic mechanisms for minimizing energy expenditure," *Regulatory, Integrative and Comparative Physiology*, vol. 233, no. 5, pp. R243-R261, 1977.

[67] R. Blickhan, "The spring-mass model for running and hopping," *Journal of Biomechanics*, vol. 22, no. 11-12, pp. 1217-1227, 1989.

[68] G. A. Cavagna, F. P. Saibene, and R. Margaria, "Mechanical work in running," *Journal of Applied Physiology*, vol. 19, no. 2, pp. 249-256, 1964.

[69] C. T. Farley and O. Gonzalez, "Leg stiffness and stride frequency in human running," *Journal of Biomechanics*, vol. 29, no. 2, pp. 181-186, 1996.

[70] M. G. Pandy, "Simple and complex models for studying muscle function in walking," *Philosophical Transactions of the Royal Society B: Biological Sciences*, vol. 358, no. 1437, pp. 1501-1509, 1989.

[71] H. Geyer, A. Seyfarth, and R. Blickhan, "Compliant leg behaviour explains basic dynamics of walking and running," *Proceedings of the Royal Society B: Biological Sciences*, vol. 273, no. 1603, pp. 2861-2867, 2006.

[72] G. S. Sawicki, C. L. Lewis, and D. P. Ferris, "It pays to have a spring in your step," *Exercise and Sport Sciences Reviews*, vol. 37, no. 3, pp. 130-138, 2009.

[73] Y. Nubar and R. Contini, "A minimal principle in biomechanics," *The bulletin of mathematical biophysics*, vol. 23, pp. 377-391, 1961.

[74] W. A. Sparrow and K. M. Newell, "Metabolic energy expenditure and the regulation of movement economy," *Psychonomic Bulletin & Review*, vol. 5, pp. 173-196, 1998.

[75] J. Stenum and J. T. Choi, "Neuromuscular effort predicts walk-run transition speed in normal and adapted human gaits," *Journal of Experimental Biology*, vol. 219, no. 18, pp. 2809-2813, 2016.

[76] J. Rose, J. G. Gamble, A. Burgos, J. Medeiros, and W. L. Haskell, "Energy expenditure index of walking for normal children and for children with cerebral palsy." *Developmental Medicine & Child Neurology*, vol. 32, no. 4, pp. 333-340, 1990.

[77] D. J. Keefer, W. Tseh, J. L. Caputo, K. Apperson, S. McGreal, and D. W. Morgan, "Comparison of direct and indirect measures of walking energy expenditure in children with hemiplegic cerebral palsy," *Developmental Medicine and Child Neurology*, vol. 46, no. 5, pp. 320-324, 2004.

[78] C. M. Duffy, A. E. Hill, A. P. Cosgrove, I. S. Carry, and H. K. Graham, "Energy consumption in children with spina bifida and cerebral palsy: A comparative study," *Developmental Medicine & Child Neurology*, vol. 38, no. 3, pp. 238-243, 1996.

[79] A. van den Hecke, C. Malghem, A. Renders, C. Detrembleur, S. Palumbo, and T. M. Lejeune, "Mechanical work, energetic cost, and gait efficiency in children with cerebral palsy," *Journal of Pediatric Orthopaedics*, vol. 27, no. 6, pp. 643-647, 2007.

[80] R. S. Gailey, M. A. Wenger, M. Raya, N. Kirk, K. Erbs, P. Spyropoulos, and M. S. Nash, "Energy expenditure of trans-tibia1 amputees during ambulation at self-selected pace," *Prosthetics and Orthotics International*, vol. 18, no. 2, pp. 84-91, 1994.

[81] R. L. Waters, J. Perry, D. Antonelli, and H. Hislop, "Energy cost of walking of amputees: The influence of level of amputation," *The Journal of Bone & Joint Surgery*, vol. 58, no. 1, pp. 42-46, 1976.

[82] J. J. Genin, G. J. Bastien, B. Franck, C. Detrembleur, and P. A. Willems, "Effect of speed on the energy cost of walking in unilateral traumatic lower limb amputees," *European Journal of Applied Physiology*, vol. 103, no. 6, pp. 655-663, 2008.

[83] J. M. Donn and C. Roberts, "A review of the energy expenditure of disabled locomotion with special reference to lower limb amputees," *Physiotherapy Theory and Practice*, vol. 8, no. 2, pp. 97-108, 1992.

[84] B. R. Umberger and P. E. Martin, "Mechanical power and efficiency of level walking with different stride rates," *Journal of Experimental Biology*, vol. 210, no. 18, pp. 3255-3265, 2007.

[85] G. A. Lichtwark and A. M. Wilson, "Interactions between the human gastrocnemius muscle and the Achilles tendon during incline, level and decline locomotion," *Journal of Experimental Biology*, vol. 209, no. 21, pp. 4379-4388, 2006.

[86] E. M. Arnold and S. L. Delp, "Fibre operating lengths of human lower limb muscles during walking," *Philosophical Transactions of the Royal Society B: Biological Sciences*, vol. 366, no. 1570, pp. 1530-1539, 2011.

[87] J. R. Franz, L. C. Slane, K. Rasske, and D. G. Thelen, "Non-uniform *in vivo* deformations of the human Achilles tendon during walking," *Gait and Posture*, vol. 41, no. 1, pp. 192-197, 2015.

[88] A. L. Hof, J. P. Van Zandwijk, and M. F. Bobbert, "Mechanics of human triceps surae muscle in walking, running and jumping," *Acta Physiologica Scandinavica*, vol. 174, no. 1, pp. 17-30, 2002.

[89] T. F. Novacheck, "The biomechanics of running," *Gait & Posture*, vol. 7, no. 1, pp. 77-95, 1998.

[90] T. J. Roberts, R. L. Marsh, P. G. Weyand, and C. R. Taylor, "Muscular force in running turkeys: The economy of minimizing work," *Science*, vol. 275, no. 5303, pp. 1113-1115, 1997.

[91] D. A. Winter, “Energy generation and absorption at the ankle and knee during fast, natural, and slow cadences,” *Clinical Orthopaedics Related Research*, vol. 175, pp. 147-154, 1983.

[92] K. Kubo, Y. Kawakami, H. Kanehisa, T. Fukunaga, “Measurement of viscoelastic properties of tendon structures in vivo,” *Scandinavian Journal of Medicine & Science in Sports*, vol. 12, no. 1, pp. 3-8, 2002.

[93] G. A. Cavagna, F. P. Saibene, and R. Margaria, “Effect of negative work on the amount of positive work performed by an isolated muscle,” *Journal of Applied Physiology*, vol. 20, no. 1, pp. 157-158, 1965.

[94] U. Svantesson, B. Ernstoff, P. Bergh, and G. Grimby, “Use of a Kin-Com dynamometer to study the stretch-shortening cycle during plantar flexion,” *European Journal of Applied Physiology and Occupational Physiology*, vol. 62, pp. 415-419, 1991.

[95] J. Rubenson, D. B. Heliams, S. K. Maloney, P. C. Withers, D. G. Lloyd, and P. A. Fournier, “Reappraisal of the comparative cost of human locomotion using gait-specific allometric analyses,” *Journal of Experimental Biology*, vol. 210, no. 20, pp. 3513-3524, 2007.

[96] H. J. Ralston, “Energy-speed relation and optimal speed during level walking,” *European Journal of Applied Physiology*, vol. 17, pp. 277-283, 1958.

[97] M. Y. Zarrugh and C. W. Radcliffe, “Predicting metabolic cost of level walking,” *European Journal of Applied Physiology and Occupational Physiology*, vol. 38, pp. 215-223, 1978.

[98] K. G. Holt, S. F. Jeng, R. Ratcliffe, and J. Hamill, “Energetic cost and stability during human walking at the preferred stride frequency,” *Journal of Motor Behavior*, vol. 27, no. 2, pp. 164-178, 1995.

[99] D. R. Carrier *et al.*, “The energetic paradox of human running and hominid evolution,” *Current Anthropology*, vol. 25, no. 4, pp. 483-495, 1984.

[100] F. E. Grine, J. G. Fleagle, and R. E. Leakey. *The First Humans: Origin and Early Evolution of the Genus Homo*, Springer New York, NY, 2009.

[101] L. Liebenberg, “Persistence hunting by modern hunter-gatherers,” *Current Anthropology*, vol. 47, no. 6, pp. 1017-1026, 2006.

[102] D. M. Bramble and D. E. Lieberman, “Endurance running and the evolution of *Homo*,” *Nature*, vol. 432, no. 7015, pp. 345-352, 2004.

[103] S. R. Ward, C. M. Eng, L. H. Smallwood, and R. L. Lieber, “Are current measurements of lower extremity muscle architecture accurate?,” *Clinical Orthopaedics and Related Research*, vol. 467, no. 4, pp. 1074-1082, 2009.

[104] F. C. Anderson and M. G. Pandy, "Dynamic optimization of human walking," *Journal of Biomechanical Engineering*, vol. 123, no. 5, pp. 381-390, 2001.

[105] M. Ackermann and A. J. van den Bogert, "Optimality principles for model-based prediction of human gait," *Journal of Biomechanics*, vol. 43, no. 6, pp. 1055-1060, 2010.

[106] D. C. Ackland, Y. C. Lin, and M. G. Pandy, "Sensitivity of model predictions of muscle function to changes in moment arms and muscle-tendon properties: A Monte-Carlo analysis," *Journal of Biomechanics*, vol. 45, no. 8, pp. 1463-1471, 2012.

[107] C. Redl, M. Gfoehler, and M. G. Pandy, "Sensitivity of muscle force estimates to variations in muscle-tendon properties," *Human Movement Science*, vol. 26, no. 2, pp. 306-319, 2007.

[108] Y. Nam and H. W. Uhm, "Tendon slack length and its effect on muscle force-generation characteristics," *Journal of Mechanics in Medicine and Biology*, vol. 11, no. 2, pp. 445-456, 2011.

[109] L. Out, T. G. M. Vrijkotte, A. J. van Soest, and M. F. Bobbert, "Influence of the parameters of a human triceps surae muscle model on the isometric torque-angle Relationship," *Journal of Biomechanical Engineering*, vol. 118, no. 1, pp. 17-25, 1996.

[110] M. Bobbert, "Dependence of human squat jump performance on the series elastic compliance of the triceps surae: a simulation study," *Journal of Experimental Biology*, vol. 204, no. 3, pp. 533-542, 2001.

[111] M. de Zee and M. Voigt, "Moment dependency of the series elastic stiffness in the human plantar flexors measured in vivo," *Journal of Biomechanics*, vol. 34, no. 11, pp. 1399-1406, 2001.

[112] C. N. Maganaris, J. P. Paul, "Load-elongation characteristics of in vivo human tendon and aponeurosis," *Journal of Experimental Biology*, vol. 203, no. 4, pp. 751-756, 2000.

[113] M. Ito, Y. Kawakami, Y. Ichinose, S. Fukashiro, and T. Fukunaga, "Nonisometric behavior of fascicles during isometric contractions of a human muscle," *Journal of Applied Physiology*, vol. 85, no. 4, pp. 1230-1235, 1998.

[114] T. Muramatsu, T. Muraoka, D. Takeshita, Y. Kawakami, Y. Hirano, and T. Fukunaga, "Mechanical properties of tendon and aponeurosis of human gastrocnemius muscle in vivo," *Journal of Applied Physiology*, vol. 90, no. 5, pp. 1671-1678, 2001.

[115] T. Finni, J. A. Hodgson, A. M. Lai, V. Reggie Edgerton, and S. Sinha, "Nonuniform strain of human soleus aponeurosis-tendon complex during submaximal voluntary contractions in vivo," *Journal of Applied Physiology*, vol. 95, no. 2, pp. 829-2837, 2003.

[116] S. P. Magnusson, P. Aagaard, S. Rosager, P. Dyhre-Poulsen, and M. Kjaer, "Load-displacement properties of the human triceps surae aponeurosis in vivo," *Journal of Physiology*, vol. 531, no. 1, pp. 277–288, 2001.

[117] T. Delabastita, F. De Groote, and B. Vanwanseele, "Achilles tendon stiffness minimizes the energy cost in simulations of walking in older but not in young adults," *bioRxiv*, 2020.

[118] T. K. Uchida, J. L. Hicks, C. L. Dembia, and S. L. Delp, "Stretching your energetic budget: How tendon compliance affects the metabolic cost of running," *PLoS ONE*, vol. 11, no. 3, pp. 1-19, 2016.

[119] F. C. Anderson, J. M. Ziegler, M. G. Pandy, and R. T. Whalen, "Application of high-performance computing to numerical simulation of human movement," *Journal of Biomechanical Engineering*, vol. 117, no. 1, pp. 155-157, 1995.

[120] V. Q. Nguyen, R. T. Johnson, F. C. Sup, and B. R. Umberger, "Bilevel optimization for cost function determination in dynamic simulation of human gait," *IEEE Transactions on Neural Systems and Rehabilitation Engineering*, vol. 27, no. 7, pp. 1426-1435, 2019.

[121] R. H. Miller, "A comparison of muscle energy models for simulating human walking in three dimensions," *Journal of Biomechanics*, vol. 47, no. 6, pp. 1373-1381, 2014.

[122] C. L. Dembia, N. A. Bianco, A. Falisse, J. L. Hicks, and S. L. Delp, "OpenSim Moco: Musculoskeletal optimal control," *PLoS Computational Biology*, vol. 16, no. 12, pp. 1-21, 2020.

[123] F. C. Anderson and M. G. Pandy, "A dynamic optimization solution for vertical jumping in three dimensions," *Computer Methods in Biomechanics and Biomedical Engineering*, vol. 2, no. 3, pp. 201-231, 1999.

[124] M. G. Pandy, "Computer modeling and simulation of human movement," *Annual Review of Biomedical Engineering*, vol. 3, pp. 245-273, 2001.

[125] C. N. Maganaris and J. P. Paul, "*In vivo* human tendon mechanical properties," *Journal of Physiology*, vol. 521, no. 1, pp. 307-313, 1999.

[126] S. P. Magnusson *et al.*, "Differential strain patterns of the human gastrocnemius aponeurosis and free tendon, *in vivo*," *Acta Physiologica Scandinavica*, vol. 177, no. 2, pp. 185-195, 2003.

[127] P. Corrigan, J. A. Zellers, P. Balascio, K. G. Silbernagel, and D. H. Cortes, "Quantification of mechanical properties in healthy Achilles tendon using continuous shear wave elastography: A reliability and validation study," *Ultrasound in Medicine & Biology*, vol. 45, no. 7, pp. 1574-1585, 2019.

[128] J. Bercoff, M. Tanter, and M. Fink, "Supersonic shear imaging: A new technique for soft tissue elasticity mapping," *IEEE Transactions on Ultrasonics, Ferroelectrics, and Frequency Control*, vol. 51, no. 4, pp. 396-409, 2004.

[129] T. Dirrichs, V. Quack, M. Gatz, M. Tingart, C. K. Kuhl, and S. Schrading, “Shear wave elastography (SWE) for the evaluation of patients with tendinopathies,” *Academic Radiology*, vol. 23, no. 10, pp. 1204-1213, 2016.

[130] G. Ivanac *et al.*, “Importance of shear-wave elastography in prediction of Achilles tendon rupture,” *International Orthopaedics*, vol. 45, no. 4, pp. 1043-1047, 2021.

[131] S. Aubry *et al.*, “Biomechanical properties of the calcaneal tendon in vivo assessed by transient shear wave elastography,” *Skeletal Radiology*, vol. 42, no. 8, pp. 1143-1150, 2013.

[132] X.-M. Chen, L.-G. Cui, P. He, W.-W. Shen, Y.-J. Qian, and J.-R. Wang, “Shear wave elastographic characterization of normal and torn Achilles tendons: A pilot study,” *Journal of Ultrasound in Medicine*, vol. 32, no. 3, pp. 449-455, 2013.

[133] C. C. Ooi, P. Malliaras, M. E. Schneider, and D. A. Connell, “‘Soft, hard, or just right?’ Applications and limitations of axial-strain sonoelastography and shear-wave elastography in the assessment of tendon injuries,” *Skeletal Radiology*, vol. 43, no. 1, pp. 1-12, 2014.

[134] R. Prado-Costa, J. Rebelo, J. Monteiro-Barroso, and A. S. Preto, “Ultrasound elastography: compression elastography and shear-wave elastography in the assessment of tendon injury,” *Insights into Imaging*, vol. 9, no. 5, pp. 791-814, 2018.

[135] L. J. Heales *et al.*, “Shear-wave velocity of the patellar tendon and quadriceps muscle is increased immediately after maximal eccentric exercise,” *European Journal of Applied Physiology*, vol. 118, no. 8, pp. 1715-1724, 2018.

[136] C. Romer, J. Czupajllo, E. Zessin, T. Fischer, B. Wolfarth, and M. H. Lerchbaumer, “Stiffness of muscles and tendons of the lower limb of professional and semiprofessional athletes using shear wave elastography,” *Journal of Ultrasound in Medicine*, vol. 41, no. 12, pp. 3061-3068, 2022.

[137] N. Ito, H. B. Sigurðsson, R. T. Pohlig, D. H. Cortes, K. Grävare Silbernagel, and A. L. Sprague, “Reliability of continuous shear wave elastography in the pathological patellar tendon,” *Journal of Ultrasound in Medicine*, vol. 42, no. 5, pp. 1047-1055, 2023.

[138] E. J. Kuervers, C. R. Firminger, and W. B. Edwards, “Effect of knee angle and quadriceps muscle force on shear-wave elastography measurements at the patellar tendon,” *Ultrasound in Medicine and Biology*, vol. 47, no. 8, pp. 2167-2175, 2021.

[139] C. D. Peltz, J. A. Haladik, G. Divine, D. Siegal, M. van Holsbeeck, and M. J. Bey, “ShearWave elastography: repeatability for measurement of tendon stiffness,” *Skeletal Radiology*, vol. 42, no. 8, pp. 1151-1156, 2013.

[140] S. L. Delp, F. C Anderson, A. S. Arnold, P. Loan, A. Habib, C. T. John, E Guendelman, and D. G. Thelen. “OpenSim: Open-source software to create and analyze dynamic

simulations of movement," *IEEE Transactions on Biomedical Engineering*, vol. 54, no. 11, pp. 1940-1950, 2007.

[141] R. D. Crowninshield and R. A. Brand, "A physiologically based criterion of muscle force prediction in locomotion," *Journal of Biomechanics*, vol. 14, no. 11, pp. 793-801, 1981.

[142] B. R. Umberger, K. G. M. Gerritsen, and P. E. Martin, "A model of human muscle energy expenditure," *Computer Methods in Biomechanics and Biomedical Engineering*, vol. 6, no. 2, pp. 99-111, 2003.

[143] B. R. Umberger and J. Rubenson, "Understanding muscle energetics in locomotion: New modeling and experimental approaches," *Exercise and Sport Sciences Reviews*, vol. 39, no. 2, pp. 59-67, 2011.

[144] L. J. Bhargava, M. G. Pandy, and F. C. Anderson, "A phenomenological model for estimating metabolic energy consumption in muscle contraction," *Journal of Biomechanics*, vol. 37, no. 1, pp. 81-88, 2004.

[145] B. R. Umberger and G. E. Caldwell, "Musculoskeletal modeling," in *Research Methods in Biomechanics*, 2nd ed. Human Kinetics, 2013, ch. 11, pp. 247-276.

[146] S. Porsa, Y. C. Lin, and M. G. Pandy, "Direct methods for predicting movement biomechanics based upon optimal control theory with implementation in OpenSim," Annals of Biomedical Engineering, vol. 44, no. 8, pp. 2542-2557, 2016.

[147] L. F. Lee and B. R. Umberger, "Generating optimal control simulations of musculoskeletal movement using OpenSim and MATLAB," *PeerJ*, vol. 2016, no. 1, pp. 1-18, 2016.

[148] Y. C. Lin and M. G. Pandy, "Three-dimensional data-tracking dynamic optimization simulations of human locomotion generated by direct collocation," *Journal of Biomechanics*, vol. 59, pp. 1-8, 2017.

[149] M. Kelly, "An introduction to trajectory optimization: How to do your own direct collocation," *SIAM Review*, vol. 59, no. 4, pp. 849-904, 2017.

[150] A. Seth *et al.*, "OpenSim: Simulating musculoskeletal dynamics and neuromuscular control to study human and animal movement," *PLoS Computational Biology*, vol. 14, no. 7, 2018.

[151] R. T. Johnson, D. Lakeland, and J. M. Finley, "Using Bayesian inference to estimate plausible muscle forces in musculoskeletal models," *Journal of NeuroEngineering and Rehabilitation volume*, vol. 19, no. 34, 2022.

[152] G. M. Amdahl, "Validity of the single processor approach to achieving large scale computing capabilities," *Proceedings of the Joint Computer Conference*, pp.483-485.

[153] A. J. K. van Soest and L. J. R. Richard Casius, "The merits of a parallel genetic algorithm in solving hard optimization problems," *Journal of Biomechanical Engineering,* vol. 125, no. 1, pp. 141-146, 2003.

[154] J. A. E. Andersson, J. Gillis, G. Horn, J. B. Rawlings, and M. Diehl, "CasADi: A software framework for nonlinear optimization and optimal control," *Mathematical Programming Computation*, vol. 11, no. 1, pp. 1-36, 2019.

[155] F. De Groote, A. L. Kinney, A. v. Rao, and B. J. Fregly, "Evaluation of direct collocation optimal control problem formulations for solving the muscle redundancy problem," *Annals of Biomedical Engineering*, vol. 44, no. 10, pp. 2922-2936, 2016.

[156] R. H. Miller and E. R. Esposito, "Transtibial limb loss does not increase metabolic cost in three-dimensional computer simulations of human walking," *PeerJ*, vol. 9, pp. 1-28, 2021.

[157] M. A. Sherman, A. Seth, and S. L. Delp, "Simbody: Multibody dynamics for biomedical research," *Procedia IUTAM,* vol 2, pp. 241-261, 2011.

[158] A. Seth, M. Sherman, J. A. Reinbolt, and S. L. Delp, "OpenSim: A musculoskeletal modeling and simulation framework for *in silico* investigations and exchange," *Procedia IUTAM,* 2011, vol. 2, pp. 212-232, 2011.

[159] K. R. S. Holzbaur, W. M. Murray, and S. L. Delp, "A model of the upper extremity for simulating musculoskeletal surgery and analyzing neuromuscular control," *Annals of Biomedical Engineering*, vol. 33, no. 6, pp. 829-840, 2005.

[160] A. Wächter and L. T. Biegler, "On the implementation of an interior-point filter line-search algorithm for large-scale nonlinear programming," *Mathematical Programming,* vol. 106, pp. 25–57, 2006.

[161] A. J. van den Bogert, D. Blana, and D. Heinrich, "Implicit methods for efficient musculoskeletal simulation and optimal control," Procedia IUTAM, vol. 2, pp. 297-316, 2011.

[162] B. Tasseff, C. Coffrin, A. Wächter, and C. Laird, "Exploring benefits of linear solver parallelism on modern nonlinear optimization applications." *arXiv,* 2019.

[163] C. O. Lovejoy, "Evolution of human walking," *Scientific American,* vol. 259, no. 5, pp. 118-125, 1988.

[164] R. H. Crompton, L. Y. W. Weijie, M. Günther, and R. Savage "The mechanical effectiveness of erect and 'bent-hip, bent-knee' bipedal walking in *Australopithecus afarensis*," vol. 35, no. 1, pp. 55-74, 1998.

[165] D. R. Carrier, C. Anders, and N. Schilling, "The musculoskeletal system of humans is not tuned to maximize the economy of locomotion," *Proceedings of the National Academy of Sciences of the United States of America*, vol. 108, no. 46, pp. 18631-18636, 2011.

[166] M. C. O'Neill, L. F. Lee, S. G. Larson, B. Demes, J. T. Stern, and B. R. Umberger, "A three-dimensional musculoskeletal model of the chimpanzee (*Pan troglodytes*) pelvis and hind limb," *Journal of Experimental Biology*, vol. 216, no. 19, pp. 3709-3723, 2013.

[167] M. Q. Salzano, S. M. Cox, S. J. Piazza, and J. Rubenson, "American Society of Biomechanics Journal of Biomechanics Award 2017: High-acceleration training during growth increases optimal muscle fascicle lengths in an avian bipedal model," *Journal of Biomechanics*, vol. 80, pp. 1-7, 2018.

[168] T. Abe, K. Kumagai, and W. F. Brechue, "Fascicle length of leg muscles is greater in sprinters than distance runners," *Medicine and Science in Sports and Exercise*, vol. 32, no. 6, pp. 1125-1129, 2000.

[169] K. Kumagai, T. Abe, W. F. Brechue, T. Ryushi, S. Takano, and M. Mizuno, "Sprint performance is related to muscle fascicle length in male 100-m sprinters," *Journal of Applied Physiology*, vol. 88, no. 3, pp. 811-816, 2000.

[170] T. Abe, S. Fukashiro, Y. Harada, and K. Kawamoto, "Relationship Between Sprint Performance and Muscle Fascicle Length in Female Sprinters," *Journal of Physiological Anthropology and Applied Human Science*, vol. 20, no. 2, pp. 141-147, 2001.

[171] M. V. Narici and C. N. Maganaris, "Adaptability of elderly human muscles and tendons to increased loading," *Journal of Anatomy*, vol. 208, no.4, pp. 433-443, 2006.

[172] M. V. Narici, C. N. Maganaris, N. D. Reeves, and P. Capodaglio, "Effect of aging on human muscle architecture," *Journal of Applied Physiology*, vol. 95, no. 6, pp. 2229-2234, 2003.

[173] C. I. Morse, J. M. Thom, K. M. Birch, and M. V. Narici, "Changes in triceps surae muscle architecture with sarcopenia," *Acta Physiologica Scandinavica*, vol. 183, no. 3, pp. 291-298, 2005.

[174] R. L. Haupt and S. E. Haupt, "Practical genetic algorithms," *Advances in Evolutionary Algorithms*, vol. 18. Berlin, Germany: Springer, 2006.

[175] R. H. Miller, B. R. Umberger, J. Hamill, and G. E. Caldwell, "Evaluation of the minimum energy hypothesis and other potential optimality criteria for human running," *Proceedings of the Royal Society B: Biological Sciences*, vol. 279, no. 1733, pp. 1498-1505, 2012.

[176] A. D. Gidley, A. P. Marsh, and B. R. Umberger, "Performance criteria for generating predictive optimal control simulations of bicycle pedaling," *Computer Methods in Biomechanics and Biomedical Engineering*, vol. 22, no. 1, pp. 11-20, 2018.

[177] K. A. Mcdonald, J. P. Cusumano, A. Hieronymi, and J. Rubenson, "Humans trade-off energetic cost with fatigue avoidance while walking", *bioRxiv*, 2022.

[178] K. A. McDonald, J. P. Cusumano, P. Peeling, and J. Rubenson, “Multi-objective control in human walking: Insight gained through simultaneous degradation of energetic and motor regulation systems,” *Journal of the Royal Society Interface*, vol. 16, pp. 20190227.

[179] L. C. Hunter, E. C. Hendrix, and J. C. Dean, “The cost of walking downhill: Is the preferred gait energetically optimal?” *Journal of Biomechanics*, vol. 43, no. 10, pp. 1910-1915, 2010.

[180] S. Kramer, L. Johnson, J. Bernhardt, and T. Cumming, “Energy expenditure and cost during walking after stroke: A systematic review,” *Archives of Physical Medicine and Rehabilitation*, vol. 97, no. 4, pp. 619-632.e1, 2016.

[181] P. E. Martin, D. E. Rothstein, and D. D. Larish, “Effects of age and physical activity status on the speed-aerobic demand relationship of walking,” *Journal of Applied Physiology*, vol. 73, no. 1, pp. 200-206, 2022.

[182] R. Nakamichi *et al.*, “The mechanosensitive ion channel PIEZO1 is expressed in tendons and regulates physical performance,” *Science Translational Medicine*, vol. 14, no. 647, pp. 1-14, 2022.

[183] F. S. Passini *et al.*, “Shear-stress sensing by PIEZO1 regulates tendon stiffness in rodents and influences jumping performance in humans,” *Nature Biomedical Engineering*, vol. 5, no. 12, pp. 1457-1471, 2021.

[184] V. A. Tucker, “Energetic cost of locomotion in animals,” *Comparative Biochemistry and Physiology*, vol. 34, pp. 841-846, 1970.

[185] P. R. Cavanagh and K. R. Williams, “The effect of stride length variation on oxygen uptake during distance running,” *Medicine and Science in Sports and Exercise*, vol. 14, no. 1, 30-35, 1982.

[186] G. A. Lichtwark and A. M. Wilson, “Is Achilles tendon compliance optimised for maximum muscle efficiency during locomotion?,” *Journal of Biomechanics*, vol. 40, no. 8, pp. 1768-1775, 2007.

[187] J. V. Benedict, L. B. Walker, and E. H. Harris, “Stress-strain characteristics and tensile strength of unembalmed human tendon,” *Journal of Biomechanics*, vol. 1, no. 1, pp. 53-56, IN11, 57-63, 1968.

[188] S. Taş, M. R. Onur, S. Yılmaz, A. R. Soylu, and F. Korkusuz, “Shear wave elastography is a reliable and repeatable method for measuring the elastic modulus of the rectus femoris muscle and patellar tendon,” *Journal of Ultrasound in Medicine*, vol. 36, no. 3, pp. 565-570, 2017.

[189] C. L. Craig et al., “International Physical Activity Questionnaire: 12-country reliability and validity,” *Medicine & Science in Sports & Exercise*, vol. 35, no. 8, pp. 1381-1395, 2003.

[190] B. Adeyeri, S. A. Thomas, and C. J. Arellano, “A simple method reveals minimum time required to quantify steady-rate metabolism and net cost of transport for human walking,” *Journal of Experimental Biology*, vol. 225, no. 15, 2022.

[191] J. M. Brockway, “Derivation of formulae used to calculate energy expenditure in man,” *Human Nutrition. Clinical Nutrition*, vol. 41, no. 6, pp. 463-471, 1987.

[192] B. D. Luciani, D. M. Desmet, A. A. Alkayyali, J. M. Leonardis, and D. B. Lipps, “Identifying the mechanical and neural properties of the sternocleidomastoid muscles,” *Journal of Applied Physiology*, vol. 124, no. 5, pp. 1297-1303, 2018.

[193] J. M. Leonardis, D. M. Desmet, and D. B. Lipps, “Quantifying differences in the material properties of the fiber regions of the pectoralis major using ultrasound shear wave elastography,” *Journal of Biomechanics*, vol. 63, pp. 41-46, 2017.

[194] C. Payne, P. Watt, M. Cercignani, and N. Webborn, “Reproducibility of shear wave elastography measures of the Achilles tendon,” *Skeletal Radiology*, vol. 47, no. 6, pp. 779-784, 2018.

[195] R. J. DeWall, L. C. Slane, K. S. Lee, and D. G. Thelen, “Spatial variations in Achilles tendon shear wave speed,” *Journal of Biomechanics*, vol. 47, no. 11, pp. 2685-2692, 2014.

[196] S. Aubry, J. P. Nueffer, M. Tanter, F. Becce, C. Vidal, and F. Michel, “Viscoelasticity in Achilles tendonopathy: Quantitative assessment by using real-time shear-wave elastography,” *Radiology*, vol. 274, no. 3, pp. 821-829, 2015.

[197] B. K. Coombes et al., “Achilles and patellar tendinopathy display opposite changes in elastic properties: A shear wave elastography study,” *Scandinavian Journal of Medicine & Science in Sports*, vol. 28, no. 3, pp. 1201-1208, 2018.

[198] M. Y. Hsiao, Y. C. Chen, C. Y. Lin, W. S. Chen, and T. G. Wang, “Reduced patellar tendon elasticity with aging: In vivo assessment by shear wave elastography,” *Ultrasound in Medicine and Biology*, vol. 41, no. 11, pp. 2899-2905, 2015.

[199] C. M. Gulledge et al., “Shear wave elastography of the healing human patellar tendon following ACL reconstruction,” *The Knee*, vol. 26, no. 2, pp. 347-354, 2019.

[200] T. Götschi et al., “Altered regional 3D shear wave velocity patterns in youth competitive alpine skiers suffering from patellar tendon complaints – a prospective case–control study,” *European Journal of Sport Science*, vol. 23, no. 6, pp. 1068-1076, 2022.

[201] D. H. Cortes, S. M. Suydam, K. G. Silbernagel, T. S. Buchanan, and D. M. Elliott, “Continuous shear wave elastography: A new method to measure viscoelastic properties of tendons *in vivo*,” *Ultrasound in Medicine and Biology*, vol. 41, no. 6, pp. 1518-1529, 2015.

[202] E. J. Rouse, L. M. Mooney, and H. M. Herr, "Clutchable series-elastic actuator: Implications for prosthetic knee design," *The International Journal of Robotics Research*, vol. 33, no. 13, pp. 1611-1625, 2014.

[203] S. Schutz, K. Mianowski, C. Kotting, A. Nejadfard, M. Reichardt, and K. Berns, "RRLAB SEA — A highly integrated compliant actuator with minimised reflected inertia," in *2016 IEEE International Conference on Advanced Intelligent Mechatronics (AIM)*, Banff, AB, Canada, pp. 252-257, 2016.

[204] B. Convens *et al.*, "Modeling, design and test-bench validation of a semi-active propulsive ankle prosthesis with a clutched series elastic actuator," *IEEE Robotics and Automation Letters*, vol. 4, no. 2, pp. 1823-1830, 2019.

[205] E. A. Bolívar-Nieto, T. Summers, R. D. Gregg, and S. Rezazadeh, "A convex optimization framework for robust-feasible series elastic actuators," *Mechatronics*, vol. 79, p. 102635, 2021.

[206] E. A. Bolivar Nieto, S. Rezazadeh, and R. D. Gregg, "Minimizing energy consumption and peak power of series elastic actuators: A convex optimization framework for elastic element design," *IEEE/ASME Transactions on Mechatronics*, vol. 24, no. 3, pp. 1334-1345, 2019.

[207] E. Bolivar, S. Rezazadeh, T. Summers, and R. D. Gregg, "Robust optimal design of energy efficient series elastic actuators: Application to a powered prosthetic ankle," in *2019 IEEE 16th International Conference on Rehabilitation Robotics (ICORR)*, Toronto, ON, Canada, 2019, pp. 740-747.

[208] E. Bolívar, S. Rezazadeh, and R. Gregg, "A general framework for minimizing energy consumption of series elastic actuators with regeneration," in *American Society of Mechanical Engineers 2017*, p. V001T36A005.

[209] K. W. Hollander, R. Ilg, T. G. Sugar, and D. Herring, "An efficient robotic tendon for gait assistance," *Journal of Biomechanical Engineering*, vol. 128, no. 5, pp. 788-791, 2006.

[210] D. Ragonesi, S. Agrawal, W. Sample, and T. Rahman, "Series elastic actuator control of a powered exoskeleton," in *2011 Annual International Conference of the IEEE Engineering in Medicine and Biology Society*, Boston, MA, 2011, pp. 3515-3518.

[211] N. C. Karavas, N. G. Tsagarakis, and D. G. Caldwell, "Design, modeling and control of a series elastic actuator for an assistive knee exoskeleton," in *2012 4th IEEE RAS & EMBS International Conference on Biomedical Robotics and Biomechatronics (BioRob)*, Rome, Italy, 2012, pp. 1813-1819.

[212] S. Kim and J. Bae, "Force-mode control of rotary series elastic actuators in a lower extremity exoskeleton using model-inverse time delay control," *IEEE/ASME Transactions on Mechatronics*, vol. 22, no. 3, pp. 1392-1400, 2017.

[213] Y. Zhu, J. Yang, H. Jin, X. Zang, and J. Zhao, “Design and evaluation of a parallel-series elastic actuator for lower limb exoskeletons,” in *2014 IEEE International Conference on Robotics and Automation (ICRA)*, Hong Kong, China, 2014, pp. 1335-1340.

[214] G. A. Pratt and M. M. Williamson, “Series elastic actuators,” in *Proceedings 1995 IEEE/RSJ International Conference on Intelligent Robots and Systems. Human Robot Interaction and Cooperative Robots*, Pittsburgh, PA, 1995, pp. 399-406.

[215] P. V. Komi, “Relevance of in vivo force measurements to human biomechanics,” *Journal of Biomechanics*, vol. 23, no. 1, pp. 23-25, 27-35, 1990.

[216] A. K. M. Lai, A. S. Arnold, and J. M. Wakeling, “Why are antagonist muscles co-activated in my simulation? A musculoskeletal model for analysing human locomotor tasks,” *Annals of Biomedical Engineering*, vol. 45, no. 12, pp. 2762-2774, 2017.

[217] E. M. Arnold, S. R. Hamner, A. Seth, M. Millard, and S. L. Delp, “How muscle fiber lengths and velocities affect muscle force generation as humans walk and run at different speeds,” *Journal of Experimental Biology*, vol. 216, no. 11, pp. 215002160, 2013.

[218] G. G. Handsfield, C. H. Meyer, J. M. Hart, M. F. Abel, and S. S. Blemker, “Relationships of 35 lower limb muscles to height and body mass quantified using MRI,” *Journal of Biomechanics*, vol. 47, no. 3, pp. 631-638, 2014.